

**A Comparison of Models for Vertical Dynamics and Noise of  
a Railway Vehicle and Track**

**A. Wei and D.J. Thompson**

ISVR Technical Memorandum No 939

August 2004



## SCIENTIFIC PUBLICATIONS BY THE ISVR

**Technical Reports** are published to promote timely dissemination of research results by ISVR personnel. This medium permits more detailed presentation than is usually acceptable for scientific journals. Responsibility for both the content and any opinions expressed rests entirely with the author(s).

**Technical Memoranda** are produced to enable the early or preliminary release of information by ISVR personnel where such release is deemed to be appropriate. Information contained in these memoranda may be incomplete, or form part of a continuing programme; this should be borne in mind when using or quoting from these documents.

**Contract Reports** are produced to record the results of scientific work carried out for sponsors, under contract. The ISVR treats these reports as confidential to sponsors and does not make them available for general circulation. Individual sponsors may, however, authorize subsequent release of the material.

### COPYRIGHT NOTICE

(c) ISVR University of Southampton All rights reserved.

ISVR authorises you to view and download the Materials at this Web site ("Site") only for your personal, non-commercial use. This authorization is not a transfer of title in the Materials and copies of the Materials and is subject to the following restrictions: 1) you must retain, on all copies of the Materials downloaded, all copyright and other proprietary notices contained in the Materials; 2) you may not modify the Materials in any way or reproduce or publicly display, perform, or distribute or otherwise use them for any public or commercial purpose; and 3) you must not transfer the Materials to any other person unless you give them notice of, and they agree to accept, the obligations arising under these terms and conditions of use. You agree to abide by all additional restrictions displayed on the Site as it may be updated from time to time. This Site, including all Materials, is protected by worldwide copyright laws and treaty provisions. You agree to comply with all copyright laws worldwide in your use of this Site and to prevent any unauthorised copying of the Materials.

UNIVERSITY OF SOUTHAMPTON  
INSTITUTE OF SOUND AND VIBRATION RESEARCH  
DYNAMICS GROUP

**A Comparison of Models for Vertical Dynamics and  
Noise of a Railway Vehicle and Track**

by

**W. Wei and D.J. Thompson**

ISVR Technical Memorandum No: 939

August 2004

Authorised for issue by  
Professor M.J. Brennan  
Group Chairman



# Contents

<b>1 Introduction</b> .....	<b>1</b>
<b>2 Track model</b> .....	<b>1</b>
2.1 Euler beam.....	2
2.2 Timoshenko beam .....	3
<b>3 Vehicle model</b> .....	<b>5</b>
3.1 Car model .....	5
3.2 Mass-spring model .....	6
<b>4 Excitation model</b> .....	<b>7</b>
4.1 Rail joint model.....	7
4.2 Wheel flat model .....	7
4.2.1 Wheel flat initial velocity excitation model .....	7
4.2.2 Wheel flat displacement model .....	8
<b>5 The selection of model length and the number of modes</b> .....	<b>10</b>
5.1 The selection of model length .....	10
5.2 The selection of number of modes .....	10
<b>6 Vibration of wheel/rail system under excitation</b> .....	<b>12</b>
6.1 The vibration of impulse excitation .....	12
6.2 Wheel flat excitation .....	13
6.2.1 Wheel flat excitation (displacement excitation).....	13
6.2.2 Wheel flat excitation (initial velocity excitation).....	15
6.3 Comparison of two kinds of excitation model .....	16
<b>7 Mass-spring system model</b> .....	<b>17</b>
7.1 Choosing number of modes for mass-spring system .....	17
7.2 The effect of velocity on contact force (Euler beam).....	18
7.3 The effect of wheel flat length on contact force (Euler beam).....	18
7.4 The effect of velocity on wheel/rail force (Timoshenko beam).....	19
7.5 The effect of wheel flat length on wheel/rail force (Timoshenko beam).....	19
7.6 The comparison of Timoshenko beam and Euler beam .....	20
7.7 Comparison of vehicle and mass-spring model (Euler beam) .....	21
7.8 Comparison of contact force of vehicle and mass-spring model (Timoshenko beam) ..	22
7.9 Comparison of the effect of wheel flat length for car model and mass spring model ...	23
<b>8 Noise caused by rail vertical vibration</b> .....	<b>24</b>
8.1 Model for noise radiation .....	24
8.2 Wheel flat initial velocity excitation .....	25
8.2.1 Sound power predicted by wagon/Euler beam model: the effect of train speed .....	25
8.2.2 Sound power predicted by wagon/Euler beam model: the effect of wheel flat length .....	26
8.2.3 Sound power predicted by wagon/Timoshenko beam model: the effect of train speed.....	27

8.2.4 Sound power predicted by wagon/Timoshenko beam model: the effect of wheel flat length.....	28
8.3 Wheel flat displacement excitation .....	29
8.3.1 Sound power predicted by wagon/Euler beam model: the effect of train speed.....	29
8.3.2 Sound power predicted by wagon/ Euler beam model: the effect of wheel flat length.....	30
8.3.3 Sound power predicted by wagon/Timoshenko beam model: the effect of train speed.....	31
8.3.4 Sound power predicted by wagon/Timoshenko beam model: the effect of wheel flat length.....	31
8.4 Mass model .....	32
8.4.1 Sound power predicted by Mass/Euler beam model: the effect of train speed.....	32
8.4.2 Sound power predicted by Mass/Euler beam model: the effect of wheel flat length .....	33
8.4.3 Sound power predicted by Mass/Timoshenko beam model: the effect of train speed .....	34
8.4.4 Sound power predicted by Mass/ Timoshenko beam model: the effect of wheel flat length.....	35
8.5 Comparison of wheel flat initial velocity and displacement excitation .....	36
8.6 Comparison of Euler beam and Timoshenko beam .....	36
8.7 Comparison of wagon and mass model.....	37
8.8 Dipped rail joint excitation.....	37
8.8.1 Sound power predicted by vehicle/ Euler beam model: the effect of train speed ...	37
8.8.2 Sound power predicted by vehicle / Timoshenko beam model: the effect of train speed.....	38
8.8.3 Sound power predicted by vehicle / Timoshenko beam model: the effect of dipped angle .....	39
<b>9 Conclusions .....</b>	<b>40</b>
<b>10 References .....</b>	<b>41</b>
<b>Appendix .....</b>	<b>42</b>
A.1 Rail parameters.....	42
A.2 Parameters under the rail .....	42
A.3 Vehicle or mass-spring parameters .....	42

# 1 Introduction

As different divisions within railway departments traditionally have managed the vehicle and track separately, the dynamics of the track and vehicle are often studied as two relatively independent problems. For vehicle dynamics, the track is considered as either a rigid support or as an elastic foundation. But for the track dynamics, the vehicle is always treated as either a single wheel or a single bogie with two wheelsets rolling on the rail. As the axle loads and vehicle speeds increase, the cost of damage to track components and derailment risks increase substantially. This leads to a widespread interest in the investigation of dynamic interactions of vehicle and track. More refined analytical models of the track and vehicle system have, therefore, started emerging. In this report, a comprehensive dynamic analysis model for the vehicle and track coupled system is used. Since the vehicle and the railway track are symmetrical about the centreline of the track, only half of the coupled system is considered.

Two models are considered for the upper structure in the coupled system. One represents the whole vehicle, while the other represents a single wheel as a mass. In the vehicle model the vertical and pitch motion for both vehicle body and bogie are considered, but for the mass model and the wheelsets of the vehicle model only vertical motion is considered. The vehicle model with two layer suspension system has ten degrees of freedom. For a one layer suspension system vehicle, six degrees of freedom are considered. The mass model has only one degree of freedom.

For the track, simple beams on an elastic foundation are commonly used. More refined analytical models of railway track have been developed. Cai and Raymond<sup>[1]</sup> reported a model in which the track was modelled as a 40-sleeper long discretely supported system of elastic beams representing the rails and the sleepers. Zhai and Sun<sup>[2]</sup> presented a detailed model in which the track is modelled as an infinite Euler beam supported on a discrete-continuous elastic foundation consisting of three layers of rail, sleeper, and ballast. Ripke and Knothe<sup>[3]</sup> developed Zhai and Sun's<sup>[2]</sup> model. They used the Timoshenko beam formulation to model the rail and sleepers. In this report, Zhai and Sun's<sup>[2]</sup> model is used, and for the purpose of comparison of the rail model effect, a Timoshenko beam formulation is also introduced to model the rail.

As models of the track and vehicle become increasingly complicated, greater computation time is needed and the interpretation of results becomes more difficult. It is therefore useful to determine whether the more complex models should always be used or whether simpler models can be used for some classes of problem. In this report several track and vehicle models are compared in order to give some guidance for the selection of model for various problems, in particular for the response to excitation by wheel flats and dipped rail joints.

## 2 Track model

A three-layer track model has been established, which includes rail, pads, sleepers and ballast (with stiffness and damping). The track model is shown in Fig. 2.1.

In this model, the rail has been represented either by an Euler or a Timoshenko beam in order to compare the difference. The sleeper is modelled as a mass and spring with stiffness and damping. The ballast is also modelled as a mass and spring, but adjacent ballast masses are coupled by a shear spring and damping. The equations of the two types of beam are derived below. All damping is assumed to be viscous.

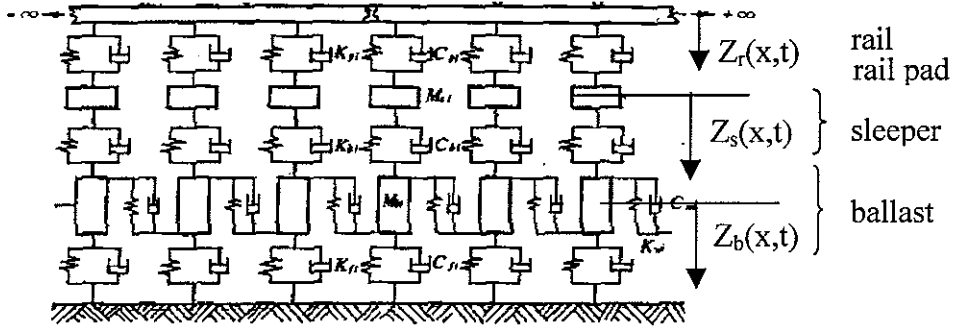


Fig. 2.1 Track model.

## 2.1 Euler beam

The notation used for the Euler beam model is:

$N$  : the number of sleepers in the model,

$E$  : young's modulus of rail,

$I$  : rail second moment of area,

$NW$  : the number of wheels.

$NM$  : the number of modes.

$F_{rsi}(t)$  : the  $i^{\text{th}}$  sleeper (pad) force acting on rail.

$G_j(t)$  : the  $j^{\text{th}}$  wheel force acting on rail.

$K_{pi}$  : stiffness of the  $i^{\text{th}}$  pad.

$C_{pi}$  : damping of the  $i^{\text{th}}$  pad.

$K_{bi}$  : stiffness of the  $i^{\text{th}}$  sleeper.

$C_{bi}$  : damping of the  $i^{\text{th}}$  sleeper.

$K_{fi}$  : stiffness of the  $i^{\text{th}}$  block of ballast.

$C_{fi}$  : damping of the  $i^{\text{th}}$  block of ballast.

$K_{wi}$  : shear stiffness between the  $i^{\text{th}}$  and  $(i+1)^{\text{th}}$  block of ballast.

$C_{wi}$  : shear damping between the  $i^{\text{th}}$  and  $(i+1)^{\text{th}}$  block of ballast.

$Z_r(x_i, t)$  : rail vertical deflection at point  $x_i$ .

$Z_{si}(t)$  : the  $i^{\text{th}}$  sleeper vertical displacement.

$Z_{bi}(t)$  : the  $i^{\text{th}}$  ballast mass vertical displacement.

$p_j(t)$  : the contact force between  $j^{\text{th}}$  wheel and rail.

$p_0$  : the static contact force between wheel and rail.

$G_c$  : contact constant of wheel and rail.

$m_r$  : rail mass per unit length.

$l$  : length of model.

$\eta(t)$  : displacement irregularity.

The equation of motion for the Euler beam<sup>[4]</sup> is:

$$EI \frac{\partial^4 Z_r(x, t)}{\partial x^4} + m_r \frac{\partial^2 Z_r(x, t)}{\partial t^2} = - \sum_{i=1}^N F_{rsi}(t) \delta(x - x_i) + \sum_{j=1}^{NW} G_j(t) \delta(x - x_{G_j}) \quad (2-1)$$

The vertical deflection  $Z_r$  is obtained using the modal superposition method, assuming a finite rail of length  $l$ .

$$\text{Set } Z_r(x, t) = \sum_{h=1}^{NM} Y_h(x) q_h(t) \quad (2-2)$$

$$\text{For a simply supported beam, the modeshapes } Y_h = \sqrt{\frac{2}{m_r l}} \sin\left(\frac{h\pi x}{l}\right) \quad (h=1,2,3\dots) \quad (2-3)$$

Multiplying equation (2-1) by  $Y_h(x)$ , and integrating from 0 to  $l$ , and utilising orthogonality equation (2-4) can be obtained.

$$\ddot{q}_h(t) + \frac{EI}{m_r} \left(\frac{h\pi}{l}\right)^4 q_h(t) = -\sum_{i=1}^N F_{rsi}(t) Y_h(x_i) + \sum_{j=1}^{NW} G_j(t) Y_h(x_{G_j}) \quad (2-4)$$

The force,  $F_{rsi}(t)$ , acting on the rail from the  $i^{\text{th}}$  pad, and  $G_j(t)$  coming from the  $j^{\text{th}}$  wheel are calculated according the following equations:

$$F_{rsi}(t) = K_{pi} [Z_r(x_i, t) - Z_{si}(t)] + C_{pi} [\dot{Z}_r(x_i, t) - \dot{Z}_{si}(t)] \quad (2-5)$$

$$G_j(t) = p_j(t) - p_0 \quad (2-6)$$

For the  $i^{\text{th}}$  sleeper, the equation of motion is:

$$M_{si} \ddot{Z}_{si}(t) = K_{pi} [Z_r(x_i, t) - Z_{si}(t)] + C_{pi} [\dot{Z}_r(x_i, t) - \dot{Z}_{si}(t)] - K_{bi} [Z_{si}(t) - Z_{bi}(t)] + C_{bi} [\dot{Z}_{si}(t) - \dot{Z}_{bi}(t)] \quad (2-7)$$

For the  $i^{\text{th}}$  ballast mass, the equation of motion is:

$$M_{bi} \ddot{Z}_{bi}(t) = C_{bi} \dot{Z}_{si}(t) + K_{bi} Z_{si}(t) + C_{wi} \dot{Z}_{b(i+1)}(t) + K_{wi} Z_{b(i+1)}(t) + C_{wi} \dot{Z}_{b(i-1)}(t) + K_{wi} Z_{b(i-1)}(t) - (K_{bi} + K_{fi} + 2K_{wi}) Z_{bi}(t) - (C_{bi} + C_{fi} + 2C_{wi}) \dot{Z}_{bi}(t) \quad (2-8)$$

where  $i$  is the number of the sleeper in the model, and  $i = 1$  to  $N$

Here the Hertz theory is used to describe the contact force and deflection of wheel and rail.

$$p_j(t) = \begin{cases} \{p_0^{2/3} + \frac{1}{G_c} [Z_{wj}(t) - Z_r(x_{G_j}, t) - \eta(t)]\}^{3/2} & \text{when wheel and rail are in contact} \\ 0 & \text{when wheel and rail are not in contact} \end{cases} \quad (2-9)$$

## 2.2 Timoshenko beam

For a Timoshenko beam the equations of motion<sup>[5]</sup> are:

$$\begin{cases} \rho A \frac{\partial^2 Z_r(x, t)}{\partial t^2} - GAk \left( \frac{\partial^2 Z_r(x, t)}{\partial x^2} - \frac{\partial \phi_r}{\partial x} \right) = -\sum_{i=1}^N F_{rsi}(t) \delta(x - x_i) + \sum_{j=1}^{NW} G_j(t) \delta(x - x_{G_j}) \\ \rho I \frac{\partial^2 \phi_r(x, t)}{\partial t^2} - GAk \left( \frac{\partial Z_r(x, t)}{\partial x} - \phi_r \right) - EI \frac{\partial^2 \phi_r(x, t)}{\partial x^2} = 0 \end{cases}$$

(2-10)

where  $Z_r$  is the vertical deflection and  $\phi_r$  is the angle of rotation of the cross section.  $G$  : shear modulus of rail,  $\rho$  : density of rail,  $A$  : cross section area of rail,  $k$  : shear coefficient of rail. The other parameters are same as for the Euler beam.

$$\text{set } \begin{cases} Z_r(x, t) = \sum_{h=1}^{NM} Y_Z(h, x) q_h(t) \\ \phi_r(x, t) = \sum_{h=1}^{NM} Y_\phi(h, x) \Phi_h(t) \end{cases} \quad (2-11)$$

A similar method to that used for the Euler beam is used here, to obtain the following equations.

$$\begin{cases} \ddot{q}_h(t) + \frac{Gk}{\rho} \left(\frac{h\pi}{l}\right)^2 q_h(t) - \sqrt{\frac{A}{I}} \frac{Gk}{\rho} \left(\frac{h\pi}{l}\right) \Phi_h = -\sum_{i=1}^N F_{rsi}(t) Y_h(x_i) + \sum_{j=1}^{NW} G_j(t) Y_h(x_{G_j}) \\ \dot{\Phi}_h + \left[\frac{GAk}{\rho I} + \frac{E}{\rho} \left(\frac{h\pi}{l}\right)^2\right] \Phi_h - \sqrt{\frac{A}{I}} \frac{Gk}{\rho} \left(\frac{h\pi}{l}\right) q_h(t) = 0 \end{cases} \quad (2-12)$$

The sleeper and ballast equations are same as that of the Euler beam.

### 3 Vehicle model

In general, the vehicle is modelled based on the various physical components, such as wheelset, bogie, body etc. Some simplified model may also be used for some special aims, for example, the mass-spring model is used for predicting high frequency vibration<sup>[7]</sup>. In this report, two kinds of vehicle model are used to predict the vibration in order to compare the difference between them. One is a vehicle with secondary suspension<sup>[4]</sup> (but no primary suspension), another is a mass-spring<sup>[7]</sup> system representing a single wheel. They are shown in Fig. 3.1 and Fig. 3.2 respectively.

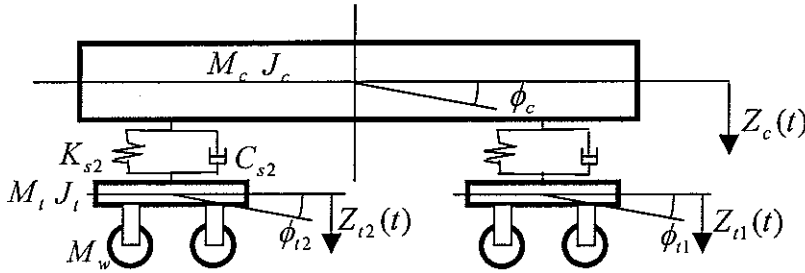


Fig. 3.1 Vehicle model.

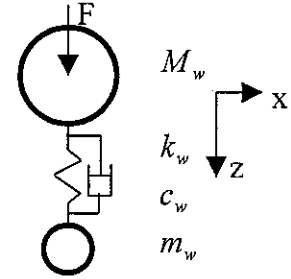


Fig. 3.2 mass-spring model.

#### 3.1 Car model

The following notation is used to describe the vehicle:

$M_c, M_t, M_w$  : mass of body, bogie and wheelset respectively.

$K_{s2}, C_{s2}$  : the stiffness and viscous damping of secondary suspension respectively.

$J_c, J_t$  : the body and bogie mass moment of inertia about horizontal axis.

$p_i$  : the force between wheel and rail.

$p_0$  : static force between wheel and rail.

$F_{0i}$  : excitation force on  $i^{\text{th}}$  wheel.

For the vehicle model 1, the equations for each part of the vehicle are:

For the bounce of the body:

$$M_c \ddot{w}_c + 2C_{s2} \dot{w}_c + 2K_{s2} w_c - C_{s2} \dot{w}_{t1} - K_{s2} w_{t1} - C_{s2} \dot{w}_{t2} - K_{s2} w_{t2} = 0 \quad (3-1)$$

for the pitch of the body

$$J_c \ddot{\phi}_c + 2C_{s2} l_c^2 \dot{\phi}_c + 2K_{s2} l_c^2 \phi_c - C_{s2} l_c \dot{w}_{t1} - K_{s2} l_c w_{t1} + C_{s2} l_c \dot{w}_{t2} + K_{s2} l_c w_{t2} = 0 \quad (3-2)$$

for the bounce of the front bogie

$$(M_t + 2M_w) \ddot{w}_{t1} + C_{s2} \dot{w}_{t1} + K_{s2} w_{t1} - C_{s2} \dot{w}_c - K_{s2} w_c - C_{s2} l_c \dot{\phi}_c - K_{s2} l_c \phi_c + p_1(t) + p_2(t) - 2p_0 = F_{01}(t) + F_{02}(t) \quad (3-3)$$

for the pitch of the front bogie

$$(J_t + 2M_w l_t^2) \ddot{\phi}_{t1} + [p_1(t) - p_2(t)] l_t = [F_{01}(t) + F_{02}(t)] l_t \quad (3-4)$$

for the bounce of the rear bogie

$$(M_t + 2M_w)\ddot{w}_{t2} + C_{s2}\dot{w}_{t2} + K_{s2}w_{t2} - C_{s2}\dot{w}_c - K_{s2}w_c + C_{s2}l_c\dot{\phi}_c + K_{s2}l_c\phi_c + p_3(t) + p_4(t) - 2p_0 = F_{03}(t) + F_{04}(t) \quad (3-5)$$

for the pitch of the rear bogie

$$(J_t + 2M_wl_t^2)\ddot{\phi}_{t2} + [p_3(t) - p_4(t)]l_t = [F_{03}(t) + F_{04}(t)]l_t \quad (3-6)$$

### 3.2 Mass-spring model

For mass-spring model, the equations are as below

$$M_w\ddot{w}_1 = F - k_w(w_1 - w_2) - c_w(\dot{w}_1 - \dot{w}_2) \quad (3-7)$$

$$m_w\ddot{w}_2 = k_w(w_1 - w_2) + c_w(\dot{w}_1 - \dot{w}_2) - p_0 \quad (3-8)$$

where  $M_w$  : unsprung mass,  $F$ : static force on wheel (vehicle body load for each wheel),  $m_w$  : fictitious mass added at contact point,  $k_w$  : spring representing high frequency modal stiffness,  $c_w$  : corresponding damping,  $w_1$  : displacement of upper mass  $M_w$  and  $w_2$  : displacement of mass  $m_w$ .

## 4 Excitation model

There are many kinds of irregularity that can excite vibration of the vehicle and track system, but not all of them excite high frequency components of wheel/rail vibration. In this report, we focus on a dipped rail joint and a wheel flat excitation model that can excite high frequency vibration of the wheel and rail.

### 4.1 Rail joint model

For a dipped rail joint, see Fig. 4.1, an initial velocity is introduced<sup>[4]</sup> to the wheel. If the total dipped angle of the joint is  $2\alpha$ , then the initial velocity is  $V_0 = 2\alpha V$ , where  $V$  is the vehicle forward speed.

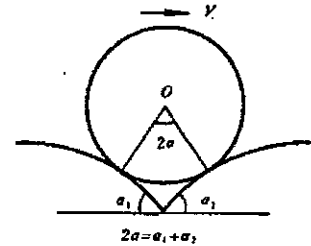


Fig. 4.1 Dipped rail joint model.

### 4.2 Wheel flat model

For the wheel flat, two models are used here. One is an initial velocity excitation model<sup>[4]</sup>, the other is a displacement excitation model<sup>[7]</sup>.

#### 4.2.1 Wheel flat initial velocity excitation model

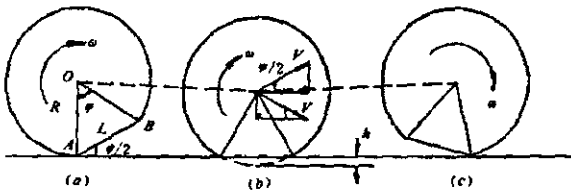


Fig. 4.2 The process of wheel flat passage on a rail at low speed.

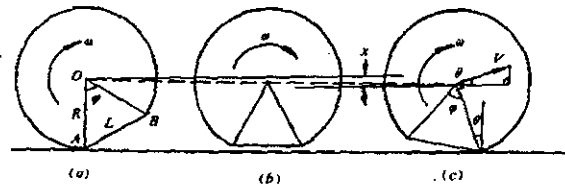


Fig. 4.3 The process of wheel flat passage on a rail at high speed.

When the wheel with the wheel flat runs at low speed, as in Fig. 4.2, the line AB (wheel flat) will contact with the rail as the wheel flat passes the contact, and after that moment, the wheel will rotate based on point B. When the speed of the vehicle is high, the line AB (wheel flat) will not contact the rail (see Fig. 4.3), because the rotation speed of the wheel is so high that the wheel centre drops less than  $h$  (height of wheel flat). It is assumed the time taken for the wheel centre to drop the distance  $h$  is  $t_1$ , and the time for the wheel to rotate an angle  $\varphi$  (corresponding to wheel flat length  $L$ ) is  $t_2$ . When  $t_1 = t_2$ , that speed is defined as the critical speed ( $V_{cr}$ ). When the vehicle speed is faster than the critical speed, the process of the wheel flat passing the rail will be like Fig. 4.3, and we call that high speed passage, otherwise we call it low speed passage.

For low speed, the impact velocity consists of two parts. The first part occurs when the flat impacts the rail when the wheel rotates around point A, and the initial vertical velocity is :

$$v_{01} = V \sin\left(\frac{\varphi}{2}\right) = V \frac{L}{2R} \quad (4-1)$$

The second part is the reaction when the wheel rotates around point B, the vertical velocity is

$$v_{02} = \gamma \frac{L}{2R} V \quad (4-2)$$

where

$V$  : vehicle speed.

$\varphi$  : the wheel flat angle.

$L$  : the length of wheel flat,

$R$  : wheel radius,

$\gamma$  : coefficient of rotation moment change into displacement moment<sup>[6]</sup>.

For high speed ( $V > V_{cr}$ ), it also consists of two parts. One is

$$v_{01} = \frac{aL}{V + \sqrt{aR}} \quad (4-3)$$

while the second part is

$$v_{02} = \frac{\gamma VL}{V + \sqrt{aR}} \sqrt{\frac{a}{R}} \quad (4-4)$$

where  $a$  is the acceleration of wheel drop, which can be calculated using the following formulation for the vehicle model.

$$a = (M_c / 4 + M_t / 2 + M_w) g / M_w \quad (4-5)$$

where  $g$  is gravity acceleration.

#### 4.2.2 Wheel flat displacement model

A wheel flat can be simulated as an initial displacement model<sup>[7]</sup>. In the model, an initial displacement is input instead of an initial velocity. Fig. 4.4 shows the model.

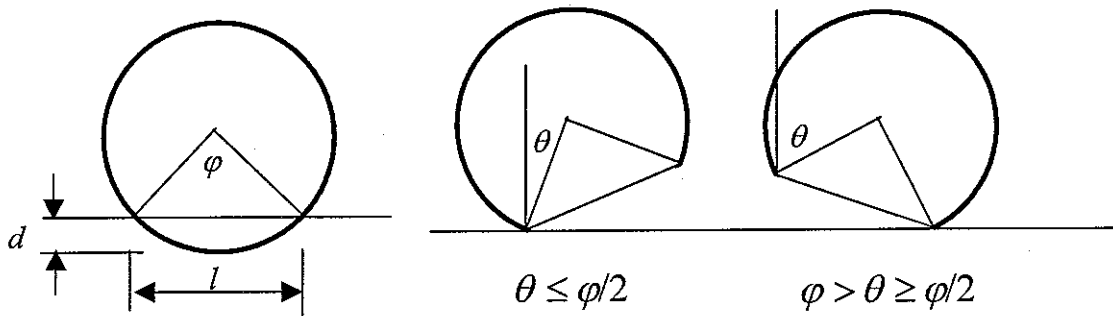


Fig. 4.4 Displacement excitation model.

The initial displacement is :

$$z = \begin{cases} r(1 - \cos \theta) & 0 \leq \theta \leq \varphi/2 \\ r[1 - \cos(\varphi - \theta)] & \varphi/2 < \theta \leq \varphi \end{cases} \quad (4-6)$$

# 5 The selection of model length and the number of modes

## 5.1 The selection of model length

The length and number of modes of the track model will affect the maximum frequency of the model. First we decide the length of the model. In vehicle dynamics calculation, a length of 3 to 4 times the vehicle length is commonly used. Here 75m, that is at least 3 times for almost any length of vehicle is selected. According to experience and a lot of results calculated with the model, it is found that a model length of 75m plus 4 times the distance between the front wheel and the rear wheel is enough for dynamics predictions.

## 5.2 The selection of number of modes

The track system consists of the rail, rail pad, ballast etc, but for rail vibration at high frequency, the pad and ballast have little effect on the rail. The rail appears therefore almost as a simply supported beam. So a simply supported beam theory is used to estimate the frequency and decide the number of modes to be included.

For an Euler beam, which is simply supported, the natural frequencies are given by

$$\omega_{nr} = \frac{r^2 \pi^2}{l^2} \sqrt{\frac{EI}{\rho A}} \quad (r=1,2,3,\dots) \quad (5-1)$$

$r$  : the mode number,  $l$  : the length of model,  $\rho$  : density of rail,  $A$  : cross section area of rail,  $E$  : Young's modulus of rail and  $I$  : rail second moment of area.

For a Timoshenko beam, the natural frequencies are the solution of

$$EI \left( \frac{r\pi}{l} \right)^4 - \rho A \omega_{nr}^2 - \rho I \left( \frac{r\pi}{l} \right)^2 \omega_{nr}^2 - \frac{\rho I E}{kG} \left( \frac{r\pi}{l} \right)^2 \omega_{nr}^2 + \frac{\rho^2 I}{kG} \omega_{nr}^4 = 0 \quad (5-2)$$

where  $k$  is the shear coefficient,  $r$  is the number of modes.

Based on equations (5-1) and (5-2), and the model length, a relation between the number of modes and the cut off frequency for different lengths and rail model are shown in Fig. 5.1 and Fig. 5.2. The parameters used are listed in the Appendix.

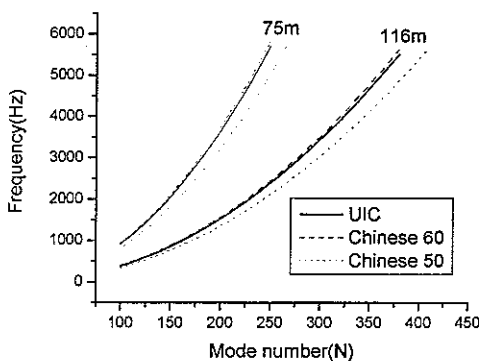


Fig. 5.1 The relation of natural frequency and modes of Euler beam.

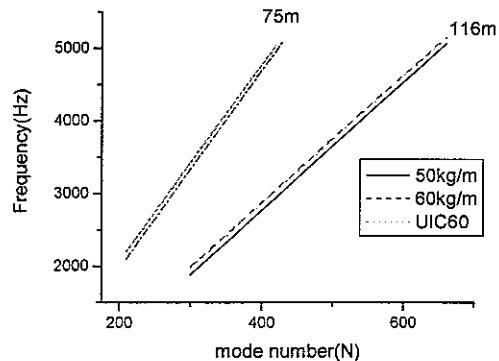


Fig. 5.2 The relation of natural frequency and modes of Timoshenko beam.

For the noise analysis, 5000Hz is the rough upper limit of frequency required, so 5000Hz is taken as the frequency limit for the beam. The table below lists the number of modes required to achieve this and the highest natural frequency obtained.

Table 1 Euler beam : the relation of number of modes and maximum frequency

Rail type	Chinese 50 kg		Chinese 60 kg		UIC60	
Rail length(m)	75	116	75	116	75	116
Number of modes	250	390	240	360	240	370
Maximum frequency (Hz)	5040	5130	5380	5060	5260	5230

Table 2 Timoshenko beam : the relation of number of modes and maximum frequency

Rail type	Chinese 50 kg		Chinese 60 kg		UIC60	
Rail length(m)	75	116	75	116	75	116
Number of modes	430	660	420	660	420	660
Maximum frequency (Hz)	5107	5063	5061	5151	5049	5139

If the number of modes is selected according to these tables, the calculation should be acceptable up to a maximum frequency of 5000Hz. For example, for a calculation of a mass-spring vehicle model on a 75m Euler beam (UIC60), 240 modes are enough for 5000Hz.

For a vehicle with the distance between front and rear wheels of 10.25m, and UIC60 rail, it needs 116m length model and 660 modes for 5000Hz.

# 6 Vibration of wheel/rail system under excitation

## 6.1 The vibration of impulse excitation

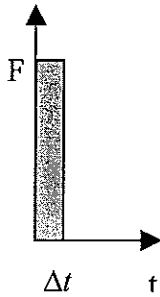


Fig. 6.1 Impulse force.

In order to analyse the difference between the Euler beam and the Timoshenko beam (UIC60), an impulse force is applied to the track system. When an impulse force is applied, the duration of the force is important to excite high frequency.

When the duration equals  $\Delta t$ , at least  $\frac{1}{\Delta t}$  Hz can be identified clearly. So for a cut off frequency of 5000Hz a force with a duration  $\Delta t = 0.0002s$  is applied. The force  $F = 100kN$  is applied.

The time domain rail displacement results are shown in Fig. 6.2. When the results are treated with the FFT method, which converts time domain results into the frequency domain, the results are as shown in Fig. 6.3

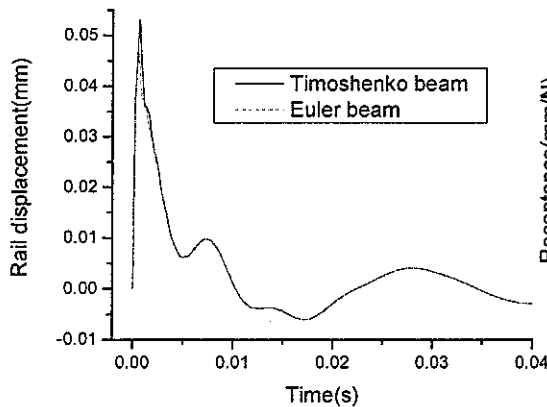


Fig. 6.2 Time domain rail displacement under impulse force.

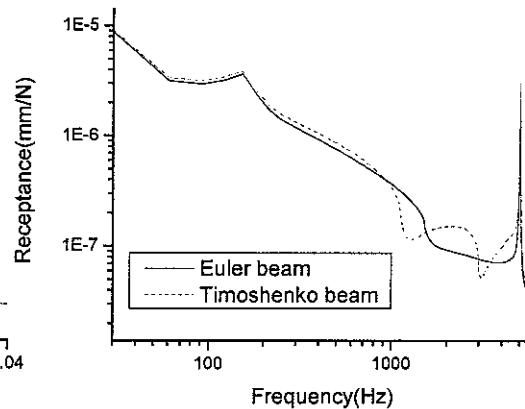


Fig. 6.3 Frequency domain rail displacement under impulse force.

From Fig. 6.2, it can be seen that, under impulse force excitation, the Euler beam and the Timoshenko beam have similar responses. At the first peak at about 0.5ms for Euler beam (0.6ms for Timoshenko beam), a notable difference can be seen in which the Timoshenko beam has about 10% greater displacement than the Euler beam. In term of the frequency responses, (see Fig. 6.3), below 900Hz the Euler beam is a little stiffer than the Timoshenko beam which can be seen from the smaller displacements under same force excitation. Around 150Hz there is a resonance for both beams. A notable difference can be seen above 900Hz. In this range the Timoshenko beam has two anti-resonances, while the Euler model has only one unclear anti-resonance at around 1500Hz. The Euler beam has only one anti-resonance as it is stiffer, and the second anti-resonance is out of the frequency range considered. So the Euler beam model will cause greater errors in high frequency vibration.

## 6.2 Wheel flat excitation

Based on the simply supported beam theory, the maximum frequency of the model is determined for a designated length. For the Timoshenko beam 660 modes are used for a maximum frequency 5000Hz. But with a track foundation it is no longer simply supported, and for particular excitation, it is found unnecessary to follow that rule. For wheel flat excitation, a series of calculations have been done in which the number of modes are reduced gradually. It is found that there is no obvious difference between the results of 660 modes and 430 modes. Fig. 6.4 is the time domain wheel/rail contact force for a speed of 30km/h for modes 660 and 430, and Fig. 6.5 is the contact force result in the frequency domain. From the time domain result it is difficult to distinguish any difference between the results of 660 modes and 430 modes. In the frequency domain result in Fig. 6.5, there is no obvious difference, except above 3000Hz where there is a small difference in amplitude between the results of 660 modes and 430 modes. So afterward in calculations for the Timoshenko beam, instead 660 modes, 430 modes have been used in the calculation. For the Euler beam 280 modes have been selected.

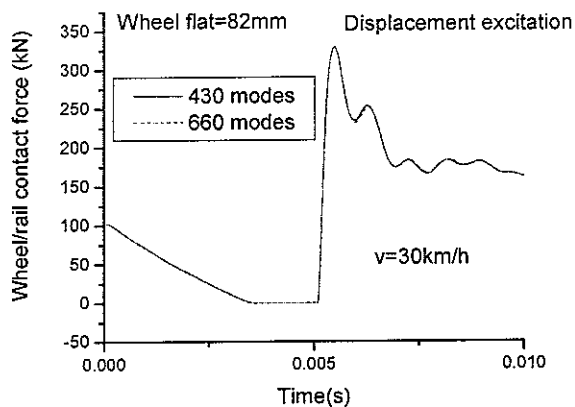


Fig. 6.4 The effect of modes number on contact force in time domain.

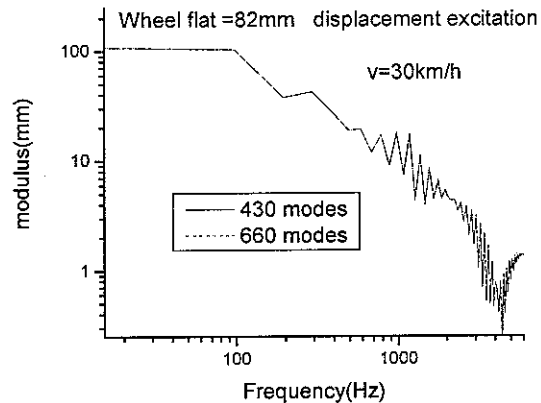


Fig. 6.5 The effect of modes number on contact force in frequency domain.

### 6.2.1 Wheel flat excitation (displacement excitation)

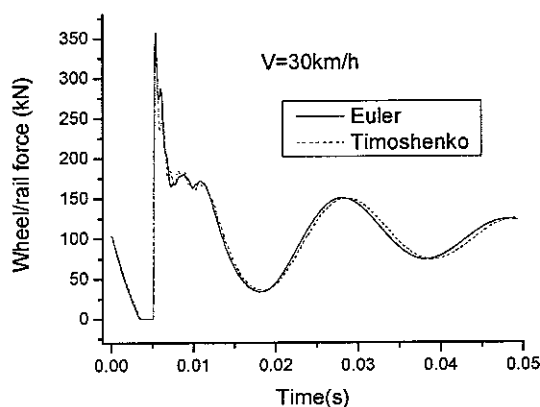


Fig. 6.6 Wheel/rail force under wheel flat displacement excitation (wheel flat length is 82mm).

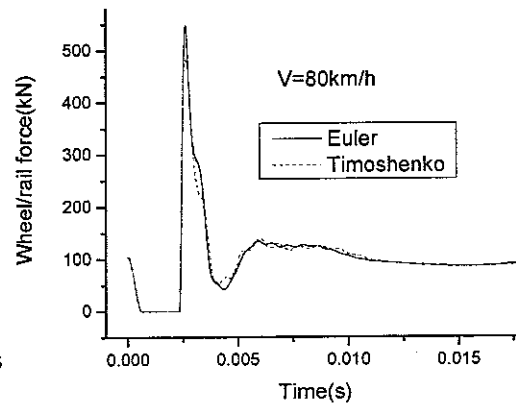


Fig. 6.7 Wheel/rail force under wheel flat displacement excitation (wheel flat length is 82mm).

Fig. 6.6 and Fig. 6.7 show the wheel/rail dynamic force under a displacement excitation with a vehicle speed of 30km/h and 80km/h respectively. Each shows the results of both Euler and Timoshenko beam models. For Euler and Timoshenko beams the force time histories are very similar except that the result of the Euler beam model has slightly larger force than the Timoshenko beam at the highest peak. When the vehicle speed is 30km/h, the largest difference in wheel/rail contact force is about 1/6 of the result from the Timoshenko model. The Euler beam is stiffer than the Timoshenko beam, so the force for the Euler beam is higher.

### 6.2.1.1 The relation of wheel/rail contact force and vehicle velocity

Calculations have been performed for the wheel flat for vehicle speeds of 30, 50, 70, 80, 90km/h. The dynamic force between wheel and rail is shown in Figs 6.8 and 6.9. From Figs 6.8 and 6.9, the effect of vehicle speed on wheel/rail contact force can be seen, in this speed range. It is can be seen that the maximum wheel/rail force increases as the vehicle speed increases.

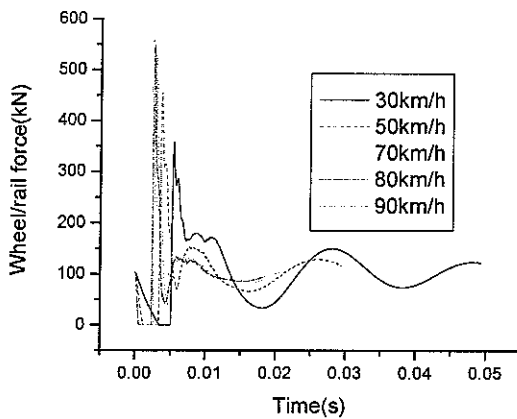


Fig. 6.8 Wheel/rail force produced by the Euler beam model.

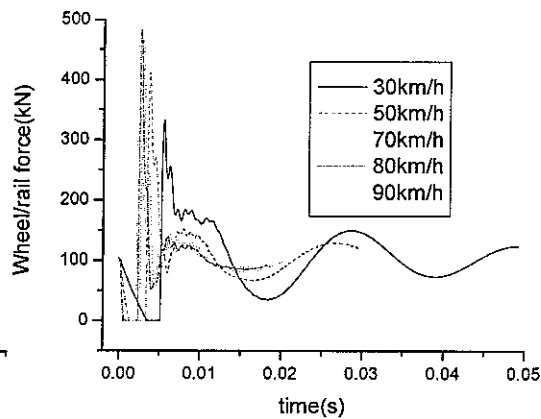


Fig. 6.9 Wheel/rail force produced by the Timoshenko beam model.

### 6.2.1.2 The effect of vehicle speed on maximum dynamic wheel/rail contact force

The relation between the peak wheel/rail contact force and vehicle velocity has been drawn in Fig. 6.10. The wheel/rail maximum contact force increases as the vehicle speed increases, but at higher speeds the increase in dynamic force slows down as the vehicle speed increases, and it will increase little when the speed is greater than 160km/h. Comparing the results of the two models, the maximum contact force of the Euler beam model is

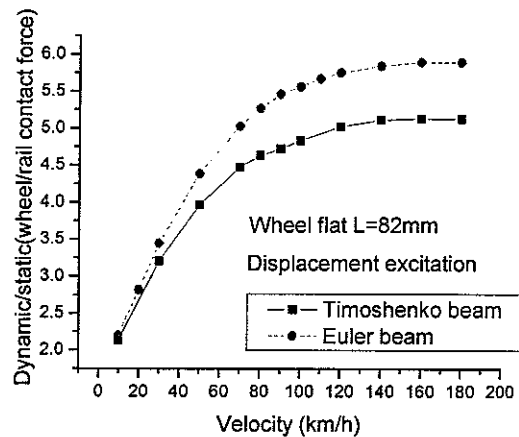


Fig. 6.10 The relation between wheel/rail force and vehicle speed.

greater than that of the Timoshenko beam model. This difference becomes larger as the speed increases. Compared with experimental results, the predicted results are about 30% greater than those of experiments<sup>[5]</sup>, so the Timoshenko beam model is better than the Euler beam model in wheel/rail dynamic force prediction.

### 6.2.2 Wheel flat excitation (initial velocity excitation)

As introduced in section 4, wheel flat excitation can be treated as a displacement excitation or transformed into an equivalent initial velocity excitation. In the previous section the displacement excitation was used but here the wheel flat is simulated using an initial velocity excitation.

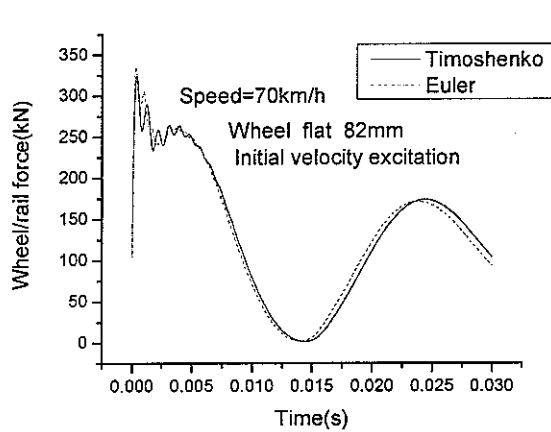


Fig. 6.11 Wheel/rail force (initial velocity excitation).

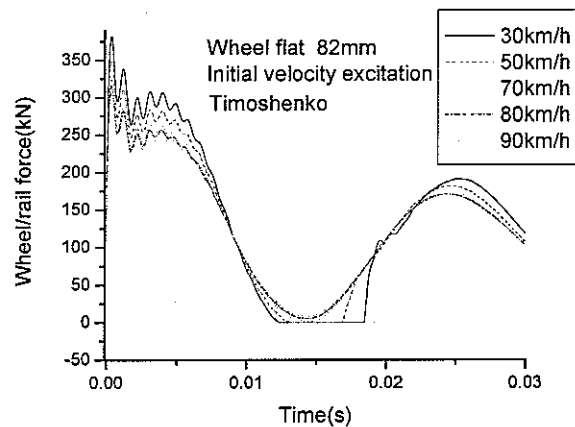


Fig. 6.12 The relation of wheel/rail force and speed (initial velocity excitation).

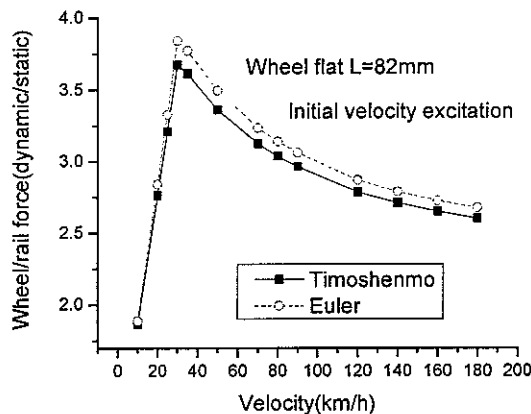


Fig. 6.13 The relation of maximum contact force and velocity.

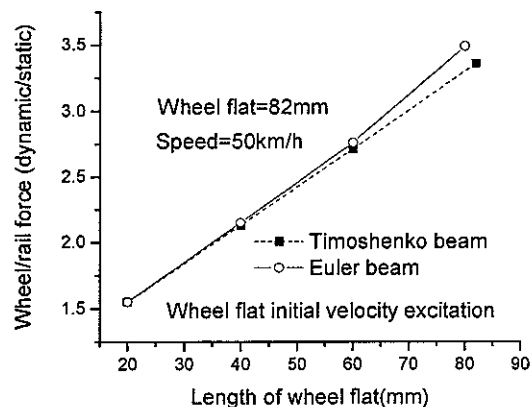


Fig. 6.14 The relation of maximum contact force and length of wheel flat.

First a wagon travelling at 70km/h is simulated. The wheel/rail contact force is shown in Fig. 6.11. Compared with displacement excitation, the wheel/rail contact force is much less for the same speed condition, especially for high train speeds. As is well known, the displacement excitation model gives an overestimate of the contact force<sup>[5]</sup>, so the initial velocity model perhaps is better to predict the wheel/rail contact

force. Another notable difference between the two excitation models is the initial velocity model has no loss of contact before the force reaches its peak, because an initial velocity is inputted instead of a wheel geometry change. At first with the initial velocity model, at low speed a large contact force occurs and after the first peak a loss of contact happens. The relation of vehicle velocity and peak contact force is shown in Fig. 6.13, from the figure, it can be seen that as the vehicle speed increases, the contact force increases and then it decreases when the velocity exceeds about 30km/h. That is very different to the displacement excitation model in which the contact force increases as the velocity increases continuously. The comparison of two beam models shows that the Euler beam produces a greater contact force than the Timoshenko beam, but the difference is smaller than that found for the displacement excitation model. With the initial velocity excitation, an effect of wheel flat length on wheel/rail contact force is shown in Fig. 6.14. From this figure, it is easy to identify that the maximum wheel/rail contact force is proportional to the length of wheel flat.

### 6.3 Comparison of two kinds of excitation model

As discussed above the two kinds of excitation model will give a different result. Here the effect of vehicle speed is shown for the two models in Fig. 6.15. The difference is particularly noticeable above 30km/h where the force continues to increase for the displacement excitation model but reduces for the initial velocity excitation model. So at high speed there will be a great difference in the predicted maximum contact force with initial velocity or displacement excitation models. For both excitation models, the Timoshenko beam's contact force is lower than that of the Euler beam. In the displacement excitation model the difference in maximum contact force of the two kinds of beam model is greater than that of initial velocity excitation.

As to the effect of wheel flat length on maximum contact force, the results are given in Figure 6.16 for a speed of 50km/h. The effect of wheel flat length is clearly seen from this figure, that contact force of wheel and rail is increased when the flat length increases, but for the displacement excitation model, the force increases more rapidly than for the initial velocity excitation model, especially at low wheel flat length.

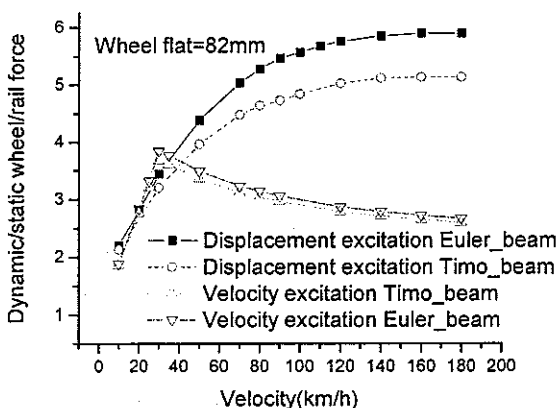


Fig. 6.15 Velocity effect on contact force of two kinds of wheel flat excitation model.

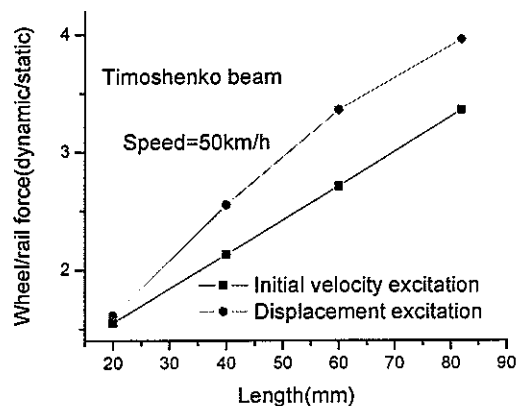


Fig. 6.16 Wheel flat length effect on contact force of two kinds of wheel flat excitation model.

# 7 Mass-spring system model

## 7.1 Choosing number of modes for mass-spring system

Some papers<sup>[7]</sup> use a mass-spring system to represent the coach to simplify the calculation. Here the results of the mass-spring model and the vehicle model are compared.

The mass-spring model is described in section 3. One mass represents the wheelset, a spring represents high frequency modal behaviour, and a small mass is introduced for numerical convergence. The model is shown in Fig. 3.2.

In the calculations the parameters are selected as below: the upper mass is 600kg, the stiffness of the spring is  $5 \times 10^9$  N/m, damping value is  $1.95 \times 10^5$  Ns/m, and the small mass is 3.0kg.

First the number of modes to be used should be determined. From equation (5-2), for a maximum frequency of 5000Hz and model length 75m, 480 modes are needed. A series of calculations have been carried each with fewer modes. Wheel flat displacement excitation is used in the calculation because it is difficult to add the velocity excitation model in the upper mass. The result of the contact force is shown in Fig. 7.1 and Fig. 7.2 for train speeds 30km/h and 80km/h.

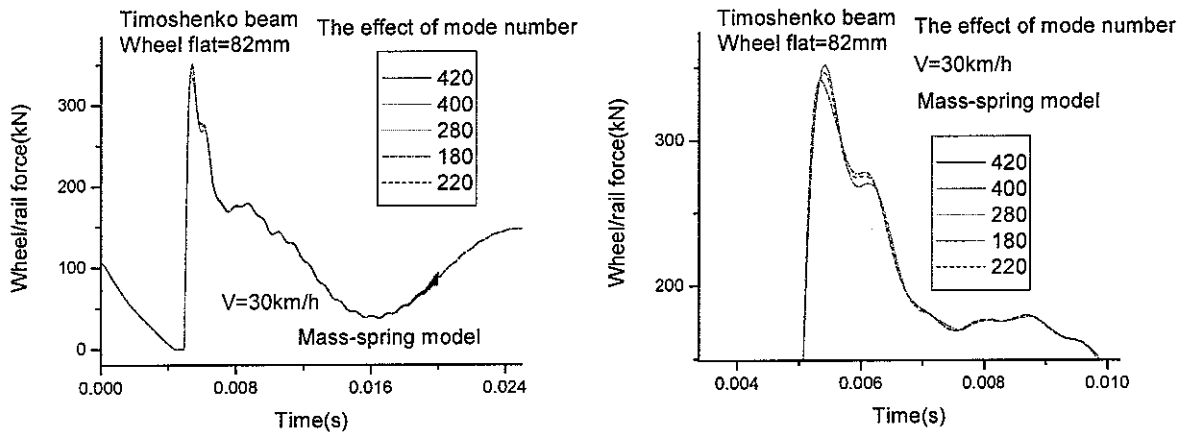


Fig. 7.1 Contact force under wheel flat excitation with different modes at velocity 30km/h.

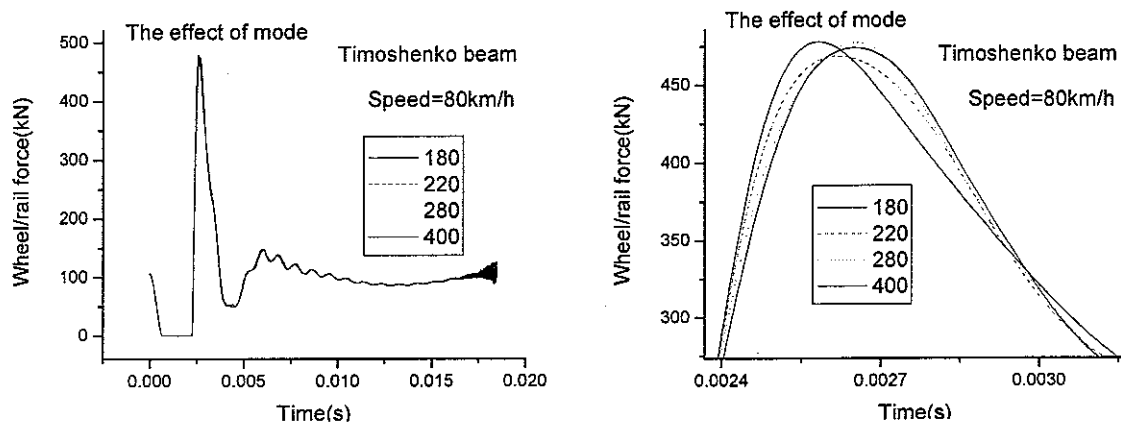


Fig. 7.2 Contact force under wheel flat excitation with different modes at speed 80km/h.

It can be seen from Figs 7.1 and 7.2, for a higher number of modes, for example 400 modes, the calculation will not converge after about 0.0175s, but for fewer modes, there are no such problems. In the series of calculations of different number of modes in the model, there is no obvious difference between the result of 280 modes and 420 modes. So 280 modes are selected for subsequent calculations.

## 7.2 The effect of velocity on contact force (Euler beam)

Fig. 7.3 shows the wheel/rail contact force when the mass model with a wheel flat passes over the Euler beam rail model with different speeds. Fig. 7.4 shows the relation between the maximum contact force and the train speed. The maximum contact force is smaller and the decay of the wheel/rail force is slower at low speed than at high speed. The maximum contact force increases as the speed increases, but for high speed the increase will slow down.

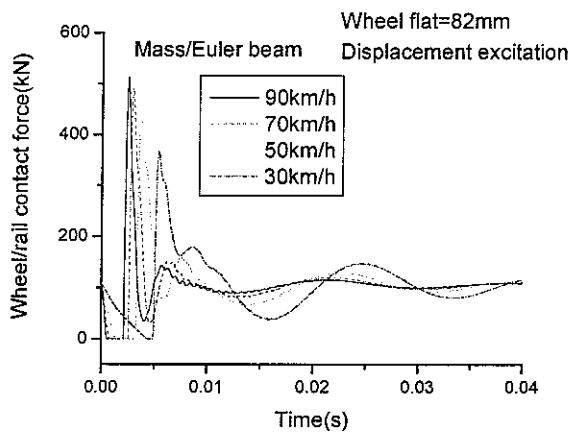


Fig. 7.3 The wheel/rail contact force under different train speed.

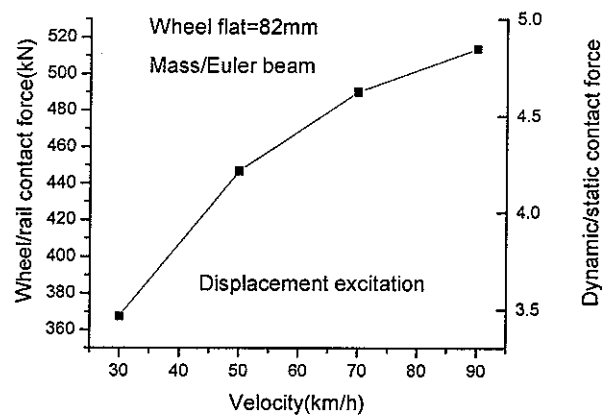


Fig. 7.4 The relation between maximum wheel/rail contact force and train speed.

## 7.3 The effect of wheel flat length on contact force (Euler beam)

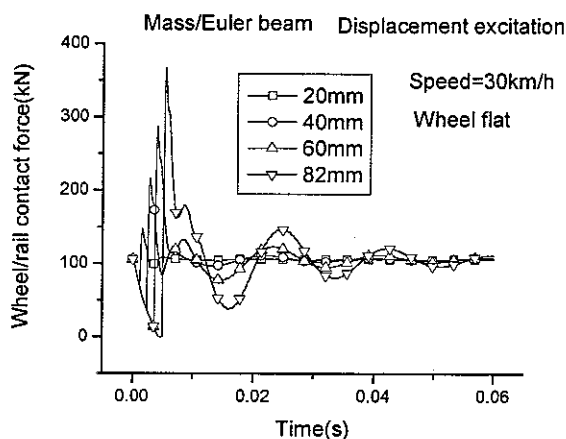


Fig. 7.5 the effect of wheel flat length on contact force.

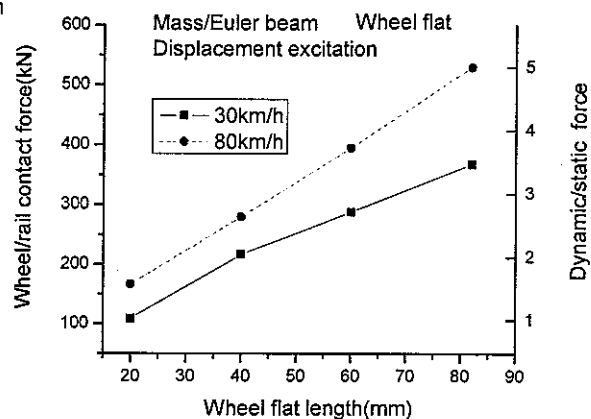


Fig. 7.6 the effect of wheel flat length on maximum contact force.

When the mass model with a wheel flat passes over the rail, the length of wheel flat may affect the amplitude of the force. Here the wheel/rail force caused by different length of wheel flat is shown in Fig. 7.5. Fig. 7.6 shows the relation of maximum contact force and wheel flat length for speed at 30km/h and 80km/h.

It is clear that the larger the wheel flat length, the higher the wheel/rail contact force. The contact force increases linearly as the length of wheel flat increases at high speed, but for low speed its increase slows down when wheel flat is large.

## 7.4 The effect of velocity on wheel/rail force (Timoshenko beam)

In this section the Euler beam is replaced by the Timoshenko beam. The wheel/rail force caused by the mass model with a wheel flat passing over the rail is shown in Fig. 7.7.

In Fig. 7.7, at first, the loss of contact happens like that in the vehicle model, and after that loss of contact, the contact force increases and reaches the peak in a very short time. For high speed, two big peaks appear obviously, but for low vehicle speed the contact force has more peaks because the vibration needs a longer time to decay to a stable value. The maximum contact force with increasing vehicle speed has been drawn in Fig. 7.8. The curve of Fig. 7.8 is very similar to that of the vehicle model in Fig. 6.10.

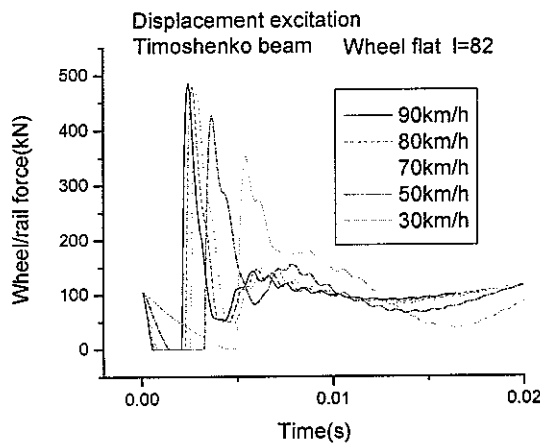


Fig. 7.7 Wheel rail contact force with wheel flat displacement excitation under different vehicle velocity.

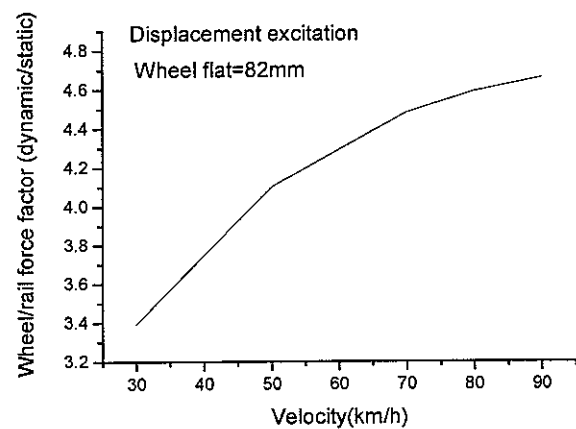


Fig. 7.8 The relation of wheel rail maximum contact force with vehicle speed under wheel flat displacement excitation.

## 7.5 The effect of wheel flat length on wheel/rail force (Timoshenko beam)

Figure 7.9 shows the effect of wheel flat length on wheel/rail contact force. From this figure, it is clear that the longer the wheel flat, the greater the contact force and loss of contact, and more time is required to return to a stable state. From Figure 7.10, it can be seen that the maximum contact force increases as the wheel flat length increases, and the relation is a straight line.

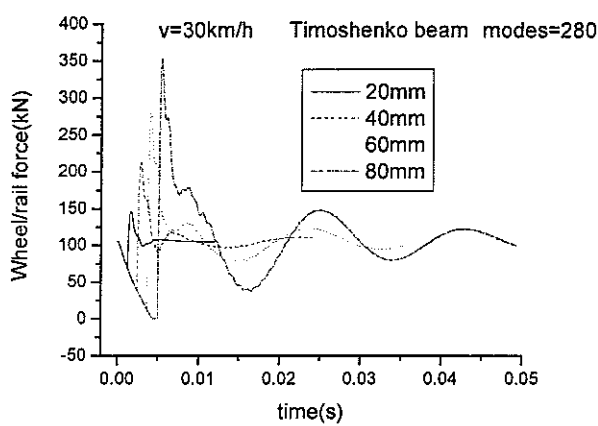


Fig. 7.9 The effect of wheel flat length on wheel rail contact force.

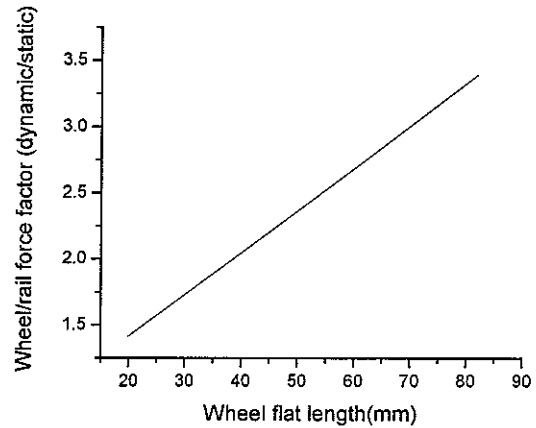


Fig. 7.10 The effect of wheel flat length on maximum wheel rail contact force at 30km/h.

## 7.6 The comparison of Timoshenko beam and Euler beam

Comparisons between the maximum contact force obtained using the Timoshenko beam and Euler beam models are shown in Figs 7.11 and 7.12. Fig. 7.11 shows the contact force for different train speeds under wheel flat displacement excitation. It is very clear that the Euler beam model predicts a higher peak force than the Timoshenko beam model at the same train speed. The difference of the contact force between the two kinds of beam increases as the speed increases, from the 7.5% at 30km/h to 14.7% at speed of 90km/h. This is very similar to the vehicle model (Figure 6.15).

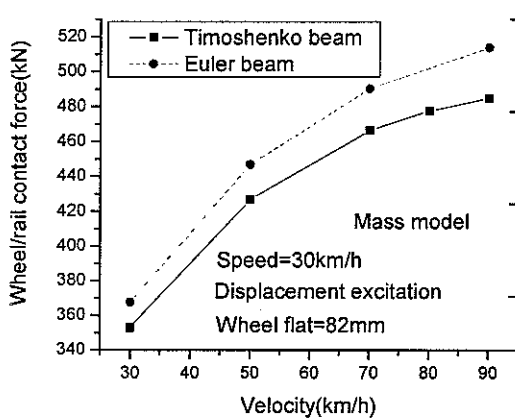


Fig. 7.11 The effect of speed on contact force for two kinds of beam.

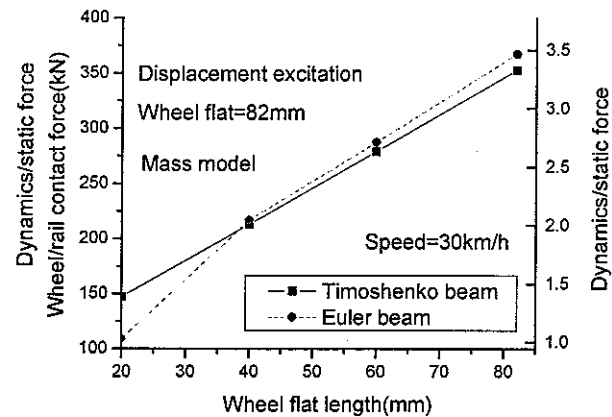


Fig. 7.12 The effect of flat length on contact force for two kinds of beam.

Fig. 7.12 shows the effect of wheel flat length on maximum contact force. It shows that at low speed (30km/h), for the middle length of wheel flat there is little difference between the Timoshenko beam and Euler beam models. However for the wheel flat length more than about 60mm, or less than 30mm, the contact force will have obvious differences.

For short wheel flat length, the Timoshenko beam model gives a higher force, but for a larger flat, the Euler beam model will predict a higher contact force than the Timoshenko beam model.

## 7.7 Comparison of vehicle and mass-spring model (Euler beam)

Figures 7.13 to 7.16 compare the results of displacements and contact forces of wheel and rail between the vehicle and mass models. The calculation condition is the Euler beam model with a speed of 30km/h and 80km/h under the wheel flat displacement excitation. From the displacement in Figures 7.13 and 7.15, it can be seen that for low train speed (Fig. 7.13) the wheel and rail displacement is slightly different for mass and vehicle model, the wheel in the mass model falls faster and deeper than that of the vehicle model, because there is no restriction for the wheel in the mass model, while for the wheel in the vehicle model the secondary suspension restricts the vibration of the wheel. But for high speed there are no distinct differences

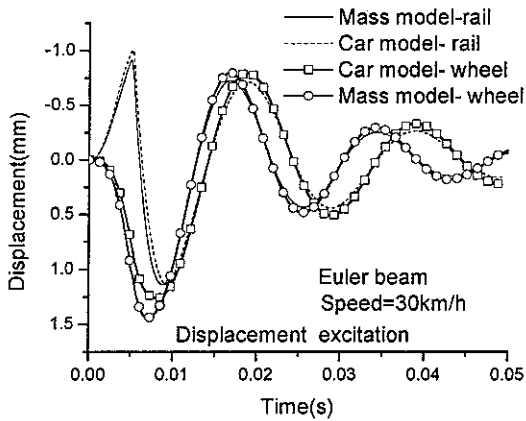


Fig. 7.13 Wheel/rail displacement for  $v=30\text{km/h}$ .

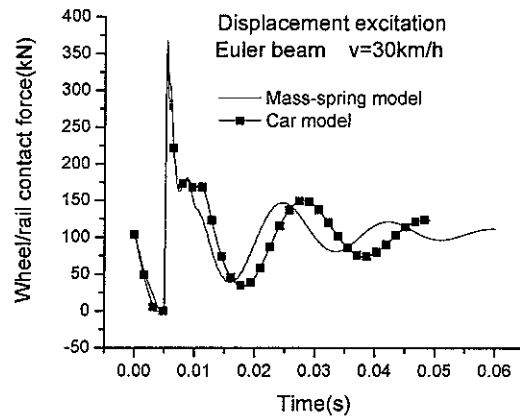


Fig. 7.14 Wheel/rail contact force for  $v=30\text{km/h}$ .

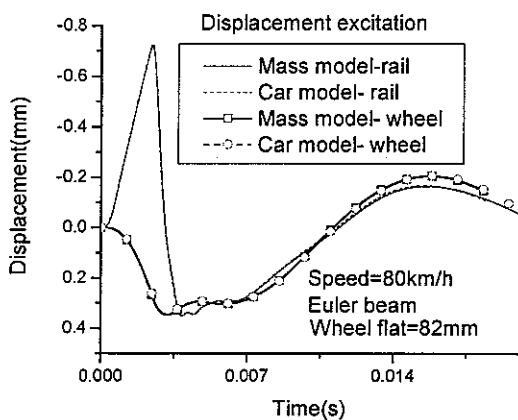


Fig. 7.15 Wheel and rail displacement for  $v=80\text{km/h}$ .

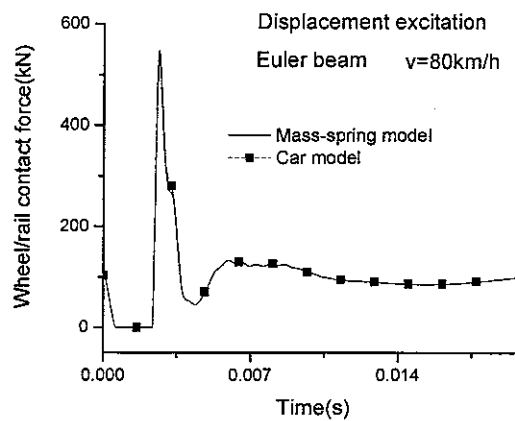


Fig. 7.16 Wheel and rail contact force for  $v=80\text{km/h}$ .

of displacement between mass and vehicle model, because there is not enough time for the wheel to fall. For the contact force, a similar conclusion can be reached, that there is little difference in contact force at high speed. That means that for high speed most of the component of vibration is at high frequency, so the mass model can be used to replace the vehicle model for high speed.

## 7.8 Comparison of contact force of vehicle and mass-spring model (Timoshenko beam)

The contact forces obtained using the vehicle and mass-spring models under wheel flat displacement excitation are shown in Figs 7.17 and 7.18 for the Timoshenko beam model.

For the aim of predicting the maximum contact force of wheel and rail, the mass-spring model gives almost the same result as the vehicle model under this particular condition. For the prediction of the vibration period, the mass-spring model gives a shorter period, because of the effect of bogie and body mass and the suspension. The vibration attenuation for mass model will be faster than that for the vehicle model, especially at the condition of low vehicle speed.

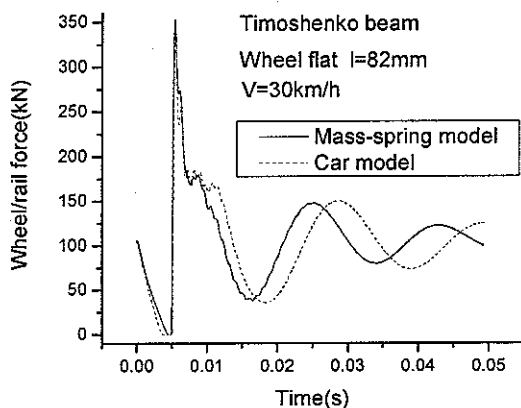


Fig. 7.17 Contact force of car and mass model under wheel flat displacement excitation at 30km/h.

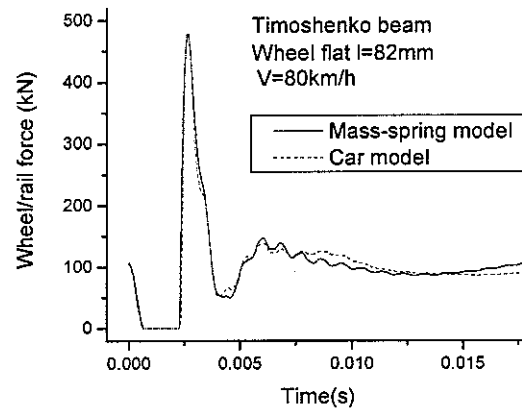


Fig. 7.18 Contact force of car and mass model under wheel flat displacement excitation at 80km/h.

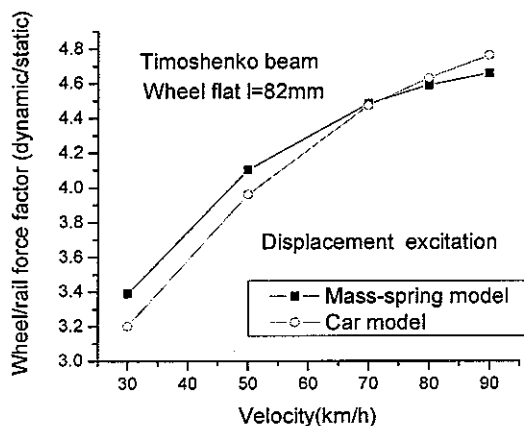


Fig. 7.19 The comparison of maximum force for mass-spring and car model.

Fig. 7.19 shows the maximum wheel/rail contact force under the wheel flat displacement excitation for mass and vehicle models. It can be seen that under some condition the two models can get almost the same result for the maximum contact force. This occurs here for a wheel flat length of 82mm at a speed of 75km/h. If mass-spring model is used to predict the wheel/rail contact force, the result is slight greater than the vehicle model at low speed, and vice versa at high speed.

## 7.9 Comparison of the effect of wheel flat length for car model and mass spring model

The relation between length of wheel flat and maximum wheel/rail contact force is shown in Figures 7.20 and 7.21 for the two vehicle models. From these figures it can be seen that the mass-spring model gives similar results to the vehicle model for short wheel flat excitation, but for longer wheel flats, it will give an error compared with the vehicle model, because the longer flat will cause lower frequency vibration while the mass model does not correctly represent the low frequency component. For the Timoshenko beam the difference is bigger between the mass and vehicle models with a longer flat than for the Euler beam model.

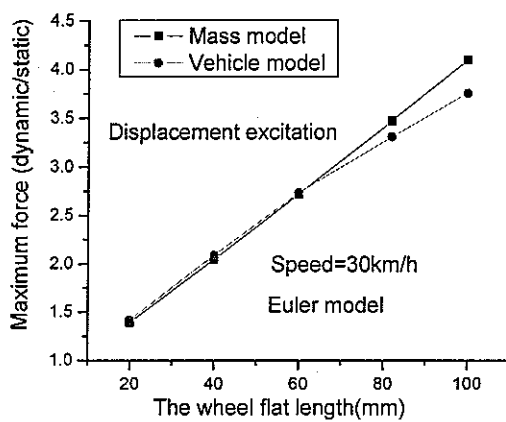


Fig. 7.20 Comparison of the effect of wheel flat length on wheel rail contact force (Euler beam).

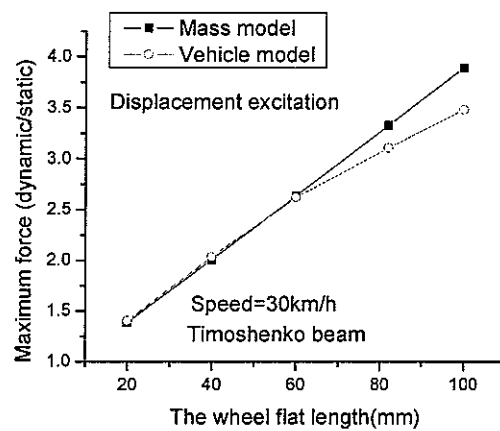


Fig. 7.21 Comparison of the effect of wheel flat length on wheel rail contact force (Timoshenko beam).

# 8 Noise caused by rail vertical vibration

## 8.1 Model for noise radiation

The aim of calculating the vibration is to predict the noise caused by the vibration. Although the lateral vibration is of the same importance as the vertical vibration for noise radiation, here only the vertical vibration of the track system is considered.

For the whole rail, the vibration velocity at many points on the rail is output in order to calculate the noise. As discussed in section 2, the vibration of the rail in the vertical direction can be expressed as a series of sine functions. To represent each sine function, at least 5 points are selected per wavelength. If  $NM$  track modes are selected in calculating the vehicle-track system vibration, the vibration at least  $2 \cdot NM + 1$  points should be output for predicting the noise.

For each output point, after the vibration velocity is output, the velocity spectrum is calculated with the FFT method. An integration of this spectrum for each 1/3-octave band is calculated to get the mean square vibration velocity corresponding to each 1/3 octave band. The data processing procedures are:

From the vehicle/track system simulation, a rail vertical vibration velocity  $v_i(t)$  is output. Here  $i$  is the number of the output point,  $i = 1 \sim 2 \cdot NM + 1$ .

For output point  $i$ , the velocity  $v_i(t)$  can be expressed as a discrete time series  $v_{ij}$ ,  $i$  and  $j$  corresponding to the output point and time step respectively.

For a discrete time series  $v_{ij}$ , its DFT is  $V_{ik}$ , given by

$$V_{ik} = \frac{1}{N} \sum_{j=0}^{N-1} v_{ij} e^{-i(2\pi k j / N)} \quad k = 0 \sim (N-1) \quad (8-1)$$

Here  $N$  is the total number of time steps.

Then the velocity spectra can be calculated by forming the products (for point  $i$ )

$$S_{v_{ik}} = V_{ik}^* V_{ik} \quad (8-2)$$

where  $V_{ik}^*$  is the complex conjugate of  $V_{ik}$

For the mean square velocity in a frequency band

$$v_{rms}^2 = 2T \int_B S_{v_{ik}} df \quad (8-3)$$

Here  $B$  is the integration range, for a 1/3-octave frequency band mean square,  $B$  is the 1/3 octave band,  $T$  is the length of the time series.

For each output point, the sound power can be calculated using the mean square vibration velocity being gained by this formula:

$$W = \rho_0 c_0 S \sigma v_{rms}^2 \quad (8-4)$$

Here  $\rho_0$  is the equilibrium density of air,  $c_0$  is the speed of sound in air,  $S$  is total radiating surface area, and  $\sigma$  is the radiation ratio.

For each output point  $i$ , the sound power is calculated using equation (8-4), where  $S$  relates to that output point, and for the whole rail, the sound power is obtained by accumulation of the power from all output points.

$$W_{total} = \sum_{i=1}^{2 \cdot NM + 1} W_i \quad (8-5)$$

Here the UIC60 rail is taken as an example. For UIC60 rail the vertical radiation section area per unit length is  $0.4\text{m}^2$ . And the length between the adjacent output points is

$$\Delta L = L / (2 * NM) \quad (8-6)$$

Here  $L$  is the model length of the rail.  $NM$  is the number of the modes.

So the radiation area in equation (8-4) becomes

$$S = 0.4 * \Delta L \quad (8-7)$$

It is convenient to express the sound power in dB, that is:

$$P = 10 \log(W_{total} / W_0) \quad (8-8)$$

Here  $W_0 = 1. \times 10^{-12}$  (W)

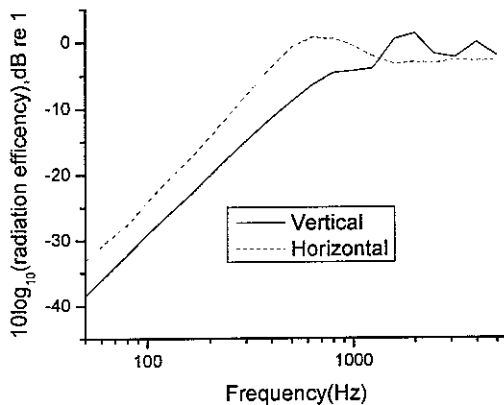


Figure 8.1 Radiation efficiency of railway rail.

In equation (8-4) the radiation ratio  $\sigma$  is very important to determine the sound power, here the radiation ratio drawn in Figure 8.1 is used<sup>[8]</sup>.

When the noise is predicted, two kinds of vehicle model are used, one is a wagon, and other is a mass model. For the track, also two kinds of model are used, Euler beam and Timoshenko beam. The details of the model are described in section 2, 3. The parameters of vehicle and track are listed in the Appendix.

## 8.2 Wheel flat initial velocity excitation

### 8.2.1 Sound power predicted by wagon/Euler beam model: the effect of train speed

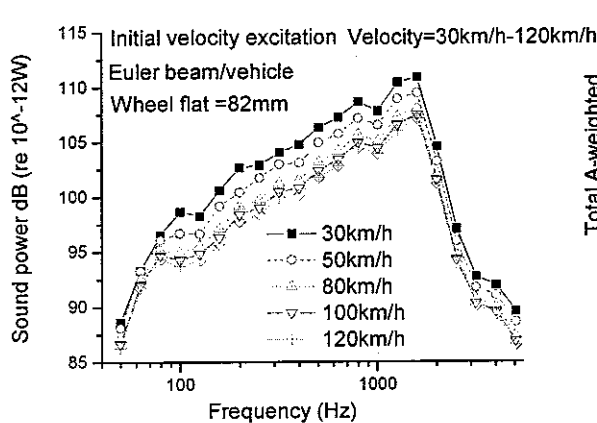


Figure 8.2 Train speed effect on sound power.

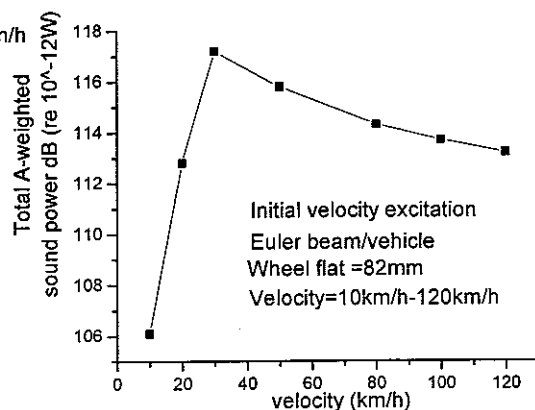


Figure 8.3 Train speed effect on total A-weighted sound power.

This section considers the noise from the rail for an Euler beam model with a wheel flat initial velocity excitation using the wagon model.

Figure 8.2 shows the sound power spectrum for different vehicle speeds under wheel flat excitation (initial velocity excitation). Figure 8.3 is the relation of total A-weighted power with the train speed.

From Figure 8.2, it can be seen, that the maximum sound power occurs at about 1600Hz for each train speed. Hence the train speed does not affect the frequency where the maximum sound power occurs. The relation of the total A-weighted sound power with train speed is shown in Fig. 8.3. The speed of maximum total A-weighted sound power occurs at 30km/h (corresponding to the maximum wheel/rail contact force). For train speeds from 30km/h to 120km/h the sound power decreases as the train speed increases over the whole frequency range, but for 80Hz-1600Hz, the change is more noticeable.

### 8.2.2 Sound power predicted by wagon/Euler beam model: the effect of wheel flat length

Figure 8.4 shows the sound power radiated by a rail for different lengths of wheel flat at speed 30km/h. Figure 8.5 is the relation between the total A-weighted sound power and the length of wheel flat.

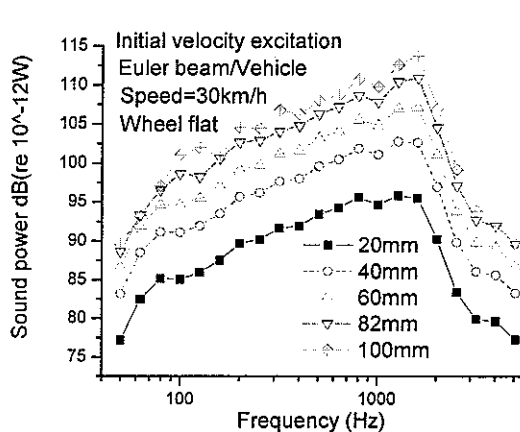


Fig. 8.4 The effect of wheel flat length on sound power.

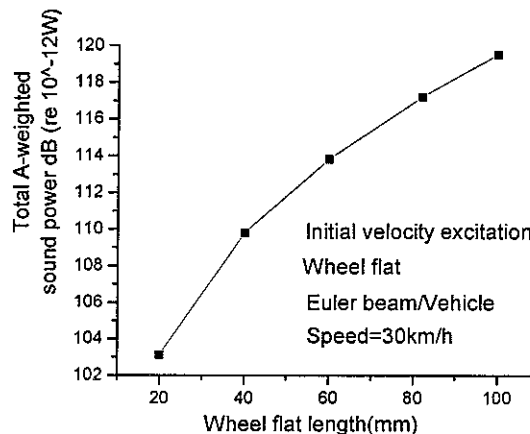


Fig. 8.5 The relation between total A-weighted sound power and wheel flat length.

It is clear that the length of the wheel flat has a certain effect on the rail noise from Fig. 8.4. All frequency components of sound power increase as the length of wheel flat increases. But for 100Hz to 1600Hz, the effect of wheel flat length is larger than in other parts of the frequency range. The sound power level increases by about 6dB for a doubling of wheel flat length. In Fig. 8.5, it can be seen the total A-weighted sound power is not a straight line, the slope of the line reduces gradually as the wheel flat length increases.

Figures 8.6 and 8.7 show the effect of length of wheel flat on sound power radiated and the relation between the total A-weighted sound power and the length of wheel flat, for a train speed of 80km/h.

From the comparison of sound power at train speeds 30km/h and 80km/h, the effect of the wheel flat length on the sound power is almost the same, except for 80km/h the sound power is smaller due to the effect of train speed seen in section 8.2.1.

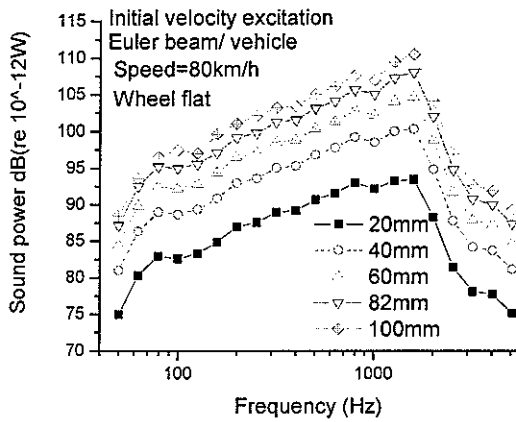


Fig. 8.6 the effect of wheel flat length on sound power.

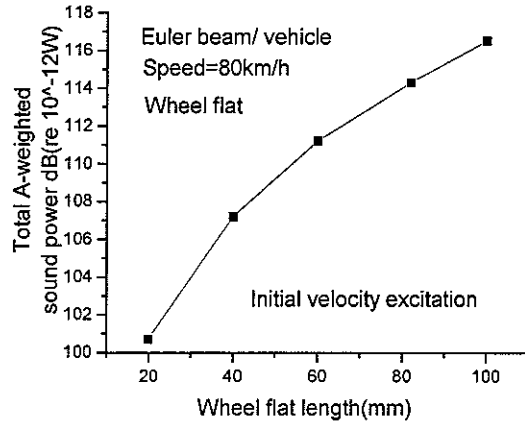


Fig. 8.7 the relation between the total A-weighted sound power and wheel flat length.

### 8.2.3 Sound power predicted by wagon/Timoshenko beam model: the effect of train speed

Figs 8.8 and 8.9 present the Timoshenko beam prediction results, for the same calculation conditions as in section 8.2.1, except the rail is represented by a Timoshenko beam instead an Euler beam.

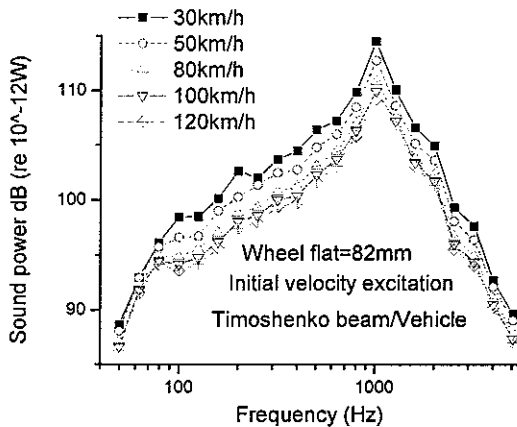


Fig. 8.8 The effect of train speed on sound power.

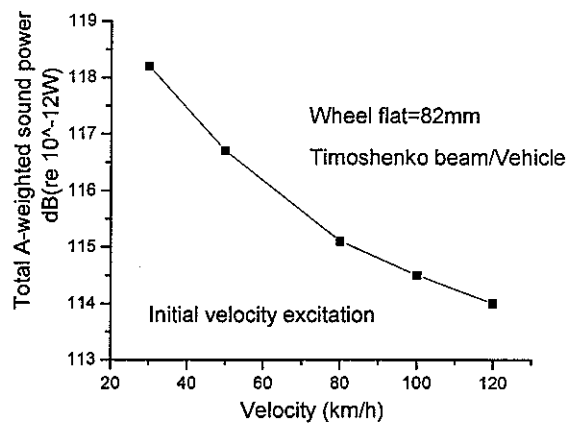


Fig. 8.9 Train speed effects on total A-weighted sound power.

The predicted sound power is different using the model of the Timoshenko beam from the Euler beam. The obvious difference is the frequency at which the maximum sound power occurs; for the Timoshenko beam it is about 1000Hz, but for the Euler beam it is 1600Hz. The main reason for the difference in frequency of maximum sound power is the Timoshenko beam is softer than the Euler beam. Moreover the Timoshenko beam model gives a greater sound power result than the Euler beam

model, for example, at 30km/h, the total A-weighted sound power is 118.2dB for the Timoshenko beam, while for the Euler beam it is 117.2dB. In the speed range from 30km/h to 120km/h, the total A-weighted sound power is about 1dB different between the Euler beam and the Timoshenko beam models.

For initial velocity excitation, the train speed does not affect the shape of the noise spectrum.

### 8.2.4 Sound power predicted by wagon/Timoshenko beam model: the effect of wheel flat length

Figs 8.10 to 8.13 show the sound power predicted by the Timoshenko beam, at train speeds 30km/h and 80km/h respectively. The calculation condition is same as section 8.2.2 except the rail taken as a Timoshenko beam.

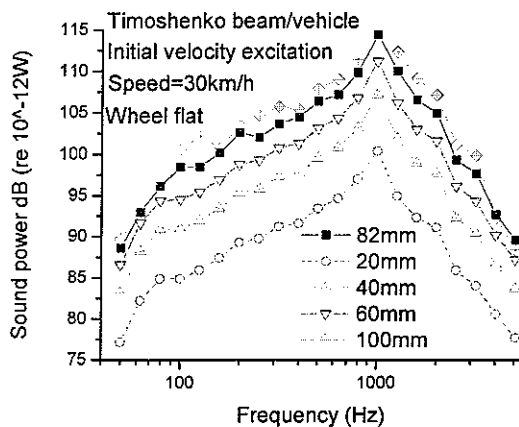


Fig. 8.10 The effect of wheel flat length on noise at speed 30km/h.

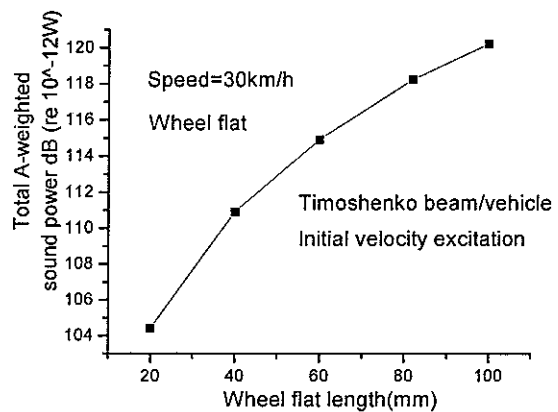


Fig. 8.11 The relation between total A-weighted sound power and wheel flat length at speed 30km/h.

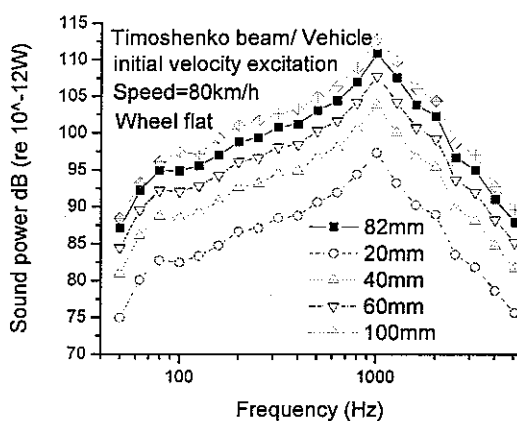


Fig. 8.12 The effect of wheel flat length on noise at speed 80km/h.

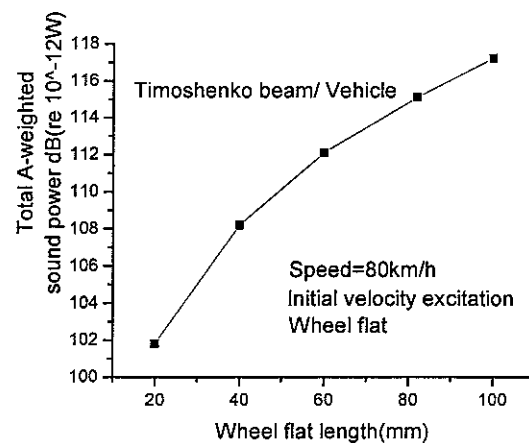


Fig. 8.13 The relation between total A-weighted sound power and wheel flat length at speed 80km/h.

From Figs 8.10 and 8.12, it is clear that the length of wheel flat will not change the frequency at which the maximum sound power occurs. For lengths in the range of

from 20 to 100mm, the maximum sound power happens at about 1000Hz. This shows again that the Timoshenko beam and the Euler beam have their maximum sound power at different frequencies.

At either 30km/h or 80km/h, the sound power will increase as the length of the wheel flat increases, and the ratio of increase is almost the same at the different speeds. The sound power level increases by about 6dB per doubling of the length.

### 8.3 Wheel flat displacement excitation

#### 8.3.1 Sound power predicted by wagon/Euler beam model: the effect of train speed

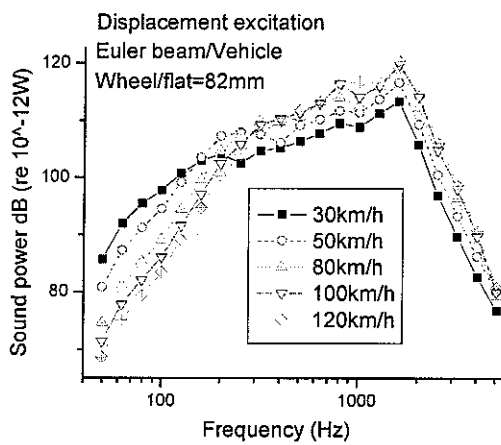


Fig. 8.14 The effect of train speed on sound power.

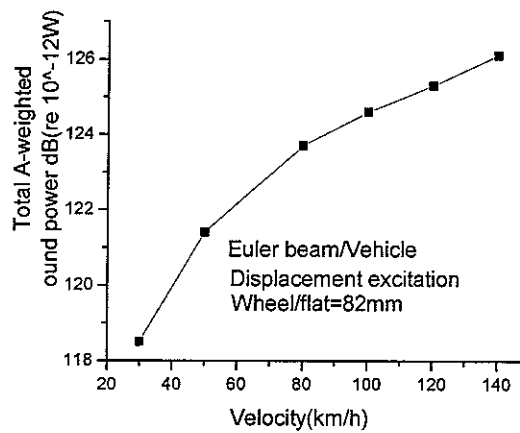


Figure 8.15 Train speed effects on the total A-weighted sound power.

Fig. 8.14 shows the predicted sound power using the Euler beam model and displacement excitation under different train speeds. Fig. 8.15 gives the relation between the total A-weighted sound power and speed. Comparing Fig. 8.14 and Fig. 8.2, it is easy to find that the frequency component of noise changes with speed for the displacement excitation model at low frequency, while in the initial velocity model, it does not change. As the speed increases, the low frequency component (especially below 200Hz) decreases. Above 200Hz, the sound power increases as the speed increases. The frequency of maximum sound power occurs again at 1600Hz that is the same as for the Euler beam model for initial velocity excitation. From Fig. 8.15, it can be seen that total A-weighted noise increases as the velocity increases. This is not the same as the results calculated by initial velocity excitation model shown in Fig. 8.3.

As to the frequency components, as the train speed increases the amount of low frequency component decreases. This is more reasonable than the initial velocity excitation model result in which the frequency components do not change as the speed changes.

### 8.3.2 Sound power predicted by wagon/ Euler beam model: the effect of wheel flat length

Fig. 8.16 shows the predicted sound power under the displacement excitation for wheel flats of different length at speed 30km/h. Fig. 8.18 is the same as Fig. 8.16 except it is for a train speed of 80km/h. Figs 8.17 and 8.19 give the effect of wheel flat length on total A-weighted sound power.

In Fig. 8.16, it can be seen, at low speed, that the noise increases when the length of wheel flat becomes larger. It is more obvious for low frequency, such as 50-200Hz, where about 35dB more noise will be produced when the length of wheel flat increases from 20mm to 100mm. However for the overall noise in Fig. 8.17 the change is not so much: it changes only by 13.9dB.

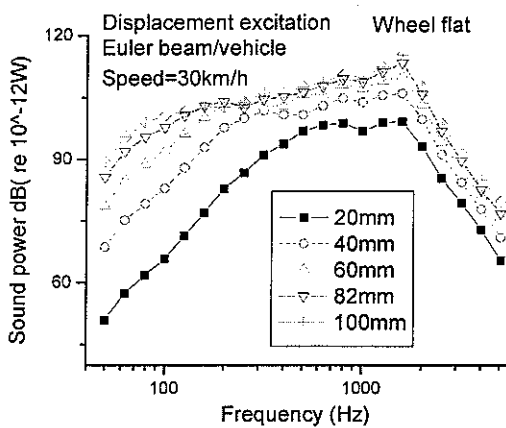


Fig. 8.16 The effect of wheel flat length on sound power.

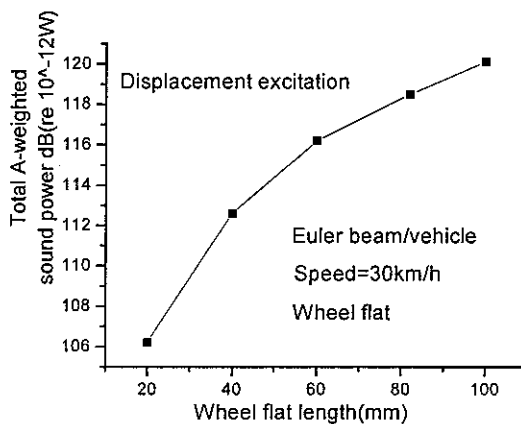


Fig. 8.17 The relation of the total A-weighted sound power and wheel flat length.

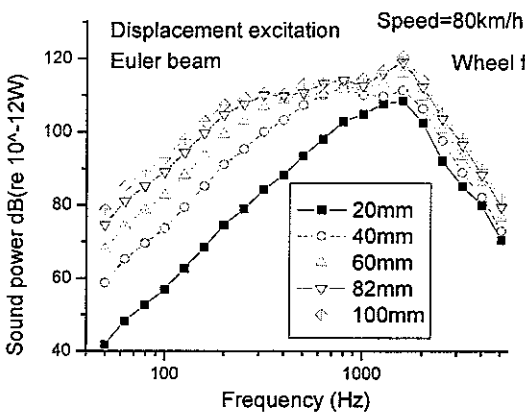


Fig. 8.18 The effect of wheel flat length on sound power.

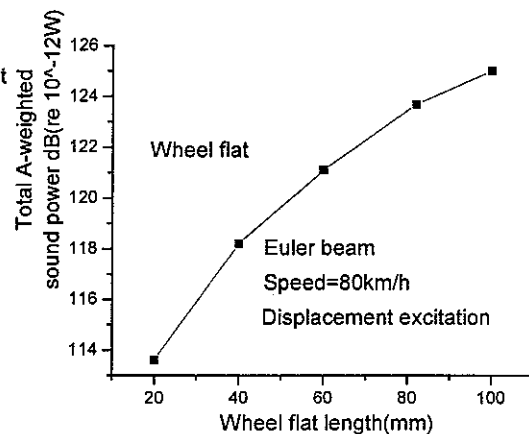


Fig. 8.19 The relation of the total A-weighted sound power and wheel flat length.

At 80km/h, the noise at low frequency again increases much more than at high frequency as the length of wheel flat increases. For 80km/h, the range of rapid increase becomes 50-300Hz. That means the noise will enhance over a broader

frequency range. The noise in this region increases about 33dB as the length of the wheel flat increases from 20mm to 100mm.

### 8.3.3 Sound power predicted by wagon/Timoshenko beam model: the effect of train speed

Figs 8.20 and 8.21 give the noise predicted by the Timoshenko beam model under wheel flat displacement excitation.

From Fig. 8.20, it can be seen that the effect of train speed on noise is very similar to the result predicted using the Euler beam (Fig. 8.14), the low frequency component noise decreases and the high frequency component noise increases when train speed increases.

Compared with the Euler beam model, the noise predicted by the Timoshenko beam has a peak at about 3000Hz that does not appear in the Euler beam model. The total A-weighted sound power is 0.4dB to 1dB more than the results predicted by the Euler beam in the velocity range of 30km/h to 120km/h.

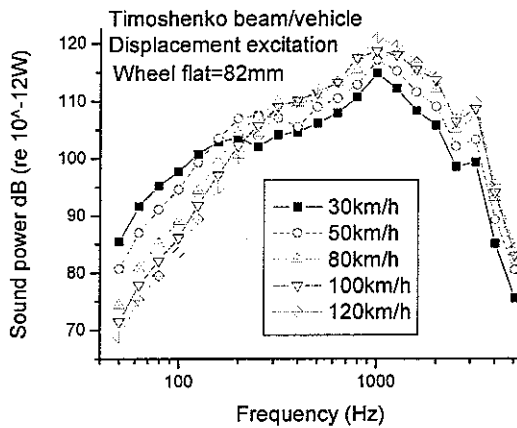


Fig. 8.20 The effect of train speed on noise.

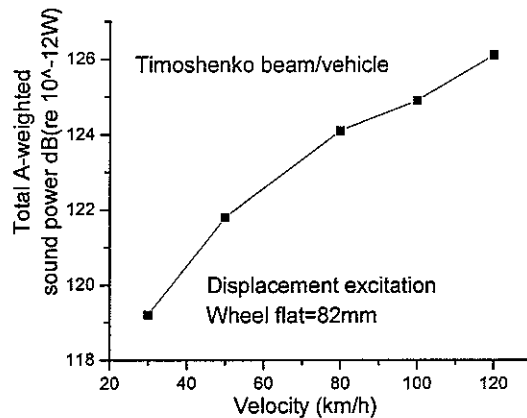


Fig. 8.21 The effect of train speed on total A-weighted sound power.

### 8.3.4 Sound power predicted by wagon/Timoshenko beam model: the effect of wheel flat length

Figs 8.22 and 8.23 give the noise predicted by the Timoshenko beam model with different wheel flat lengths at speed 30km/h. Figs 8.24 and 8.25 give the corresponding results for a train speed of 80km/h.

The results are very similar to the Euler beam results. As the length of the wheel flat becomes large the sound power will increase, and it increases rapidly at low frequency. The obvious differences between the two beam models are the frequency at which the maximum noise happens (Timoshenko beam 1000Hz, Euler beam 1600Hz) and the noise peak found for the Timoshenko beam model at around 3000Hz while the Euler beam model has no such peak.

At the speed of 30km/h when the wheel flat length is shorter, for example 20mm, the noise predicted by the Timoshenko beam is about 3dB more than that predicted by the Euler beam, but for a longer wheel flat, there is very little difference in sound power between the two beam models.

At 80km/h the effect of wheel flat length on noise reduces compared to the results at 30km/h, especially for the low frequency component of noise. That is similar with the result of the Euler beam model (see in section 8.3.2).

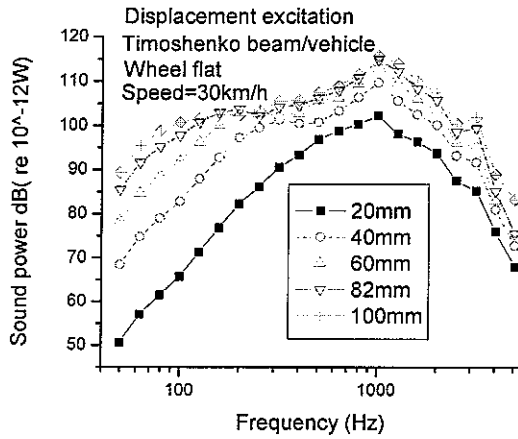


Fig. 8.22 The effect of wheel flat length on noise at speed 30km/h.

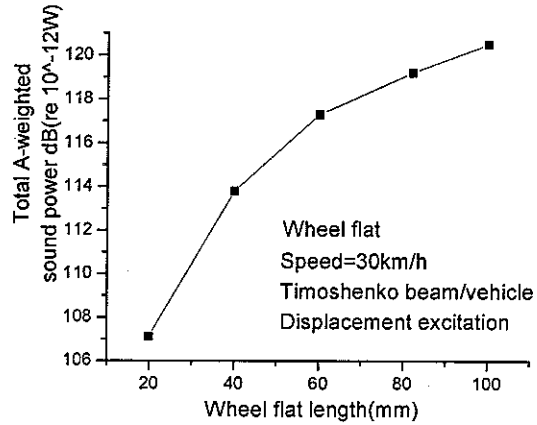


Fig. 8.23 The effect of wheel flat length on total A-weighted noise.

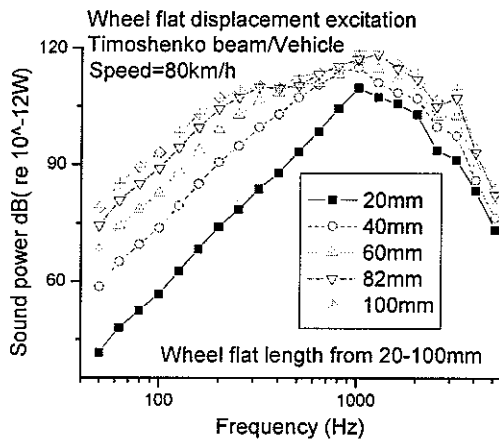


Fig. 8.24 The effect of wheel flat length on noise at speed 80km/h.

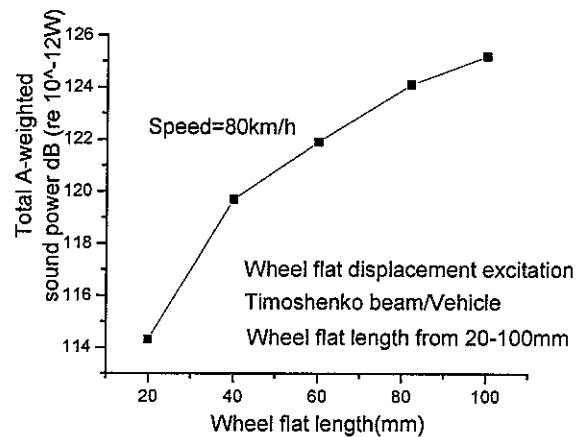


Fig. 8.25 The effect of wheel flat length on total A-weighted noise.

## 8.4 Mass model

### 8.4.1 Sound power predicted by Mass/Euler beam model: the effect of train speed

After the vehicle is replaced with the mass model, the result of noise for the Euler beam under wheel flat displacement excitation is calculated, and shown in Figs 8.26 and 8.27.

When the vehicle is replaced with the mass model, the radiated noise from the rail has no visible change except the noise has a higher level at frequency above 3000Hz.

The effect of speed on noise at low frequency and high frequency, and the change in noise between 30km/h and 120km/h, are very similar to the results already seen for the vehicle model. For the total A-weighted sound power, the results predicted by the mass model are lower by 0.4dB to 1.3dB than that for the vehicle model. The total A-weighted sound power difference is higher at high speed than that at low speed.

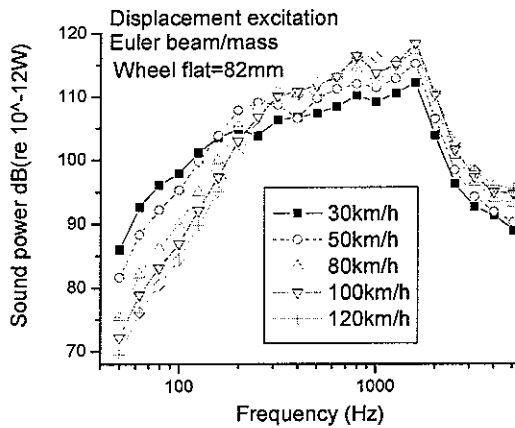


Fig. 8.26 The effect of train speed on noise with 82mm wheel flat

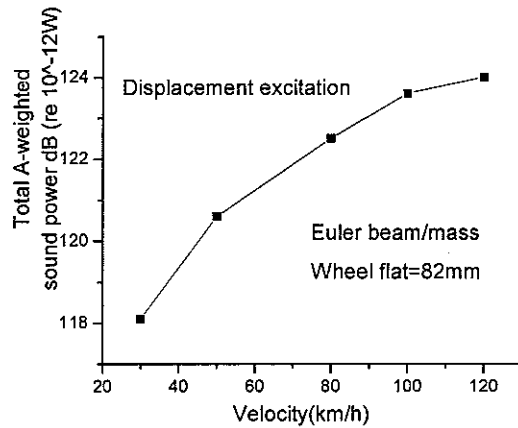


Fig. 8.27 The effect of train speed on total A-weighted noise power with 82mm wheel flat

#### 8.4.2 Sound power predicted by Mass/Euler beam model: the effect of wheel flat length

Figs 8.28 to 8.31 show the results for the mass model passing over the Euler beam rail model under the wheel flat excitation at 30km/h and 80km/h respectively.

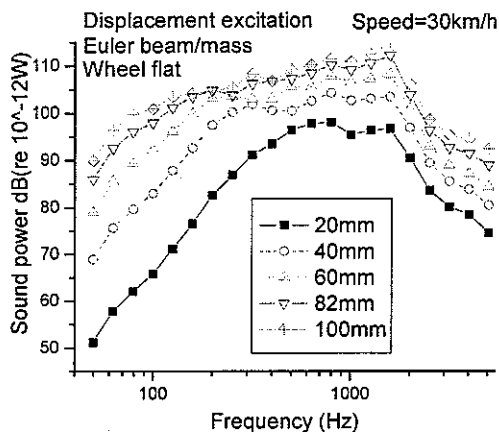


Fig. 8.28 The effect of wheel flat length on noise at speed 30km/h.

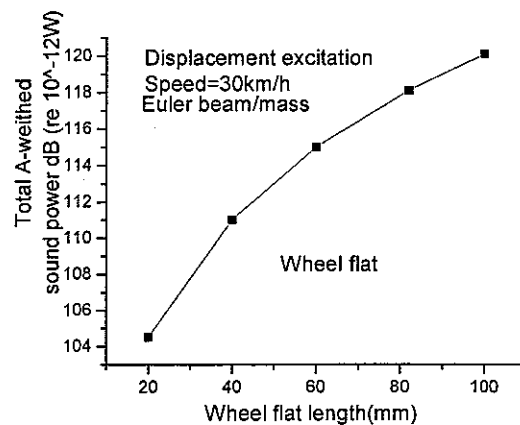


Fig. 8.29 The effect of wheel flat length on total A-weighted noise power at speed 30km/h.

The predicted noise is very similar to the vehicle model results seen in section 8.3.2. As the length of the wheel flat increases, the noise will increase, and for low frequency, (below 200Hz for 30km/h and 300Hz for 80km/h), there is a greater change as the length increases than at high frequency. At 30km/h, the noise at low frequency changes more than that at 80km/h. When the length changes from 20mm to

100mm, the total A-weighted sound power changes by 15.6dB, compared with the vehicle model where that value is 13.9dB at the same speed (30km/h).

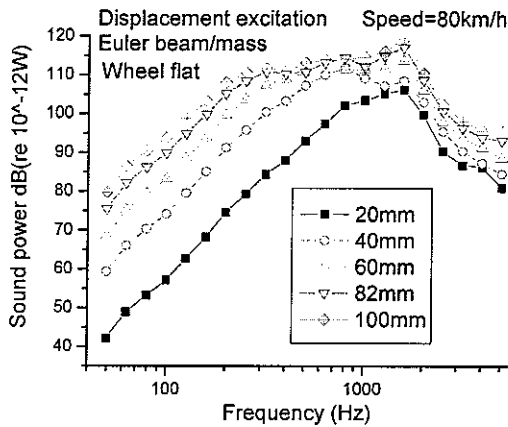


Fig. 8.30 The effect of wheel flat length on noise power at speed 80km/h.

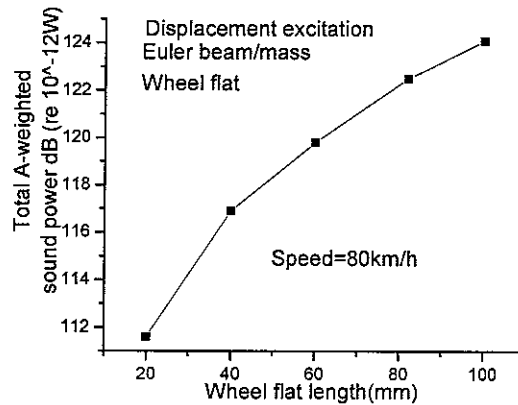


Fig. 8.31 The effect of wheel flat length on total A-weighted noise power at speed 80km/h.

### 8.4.3 Sound power predicted by Mass/Timoshenko beam model: the effect of train speed

Figs 8.32 and 8.33 show the effect of train speed on noise for the mass on the Timoshenko beam model. The excitation is a 82mm length wheel flat (displacement excitation).

Comparing Fig. 8.32 and Fig. 8.20, it is easy to see that the effect of speed on noise for the wagon model and the mass model are very similar except above 4000Hz where the noise is higher than the result predicted by the wagon model. The mass model can therefore be used to predict noise from the rail instead the vehicle model for frequencies below 4000Hz.

For the total A-weighted sound power, it is lower for the mass model than the vehicle model. The difference increases as the speed increases, it is about 0.8dB when speed is at 120km/h.

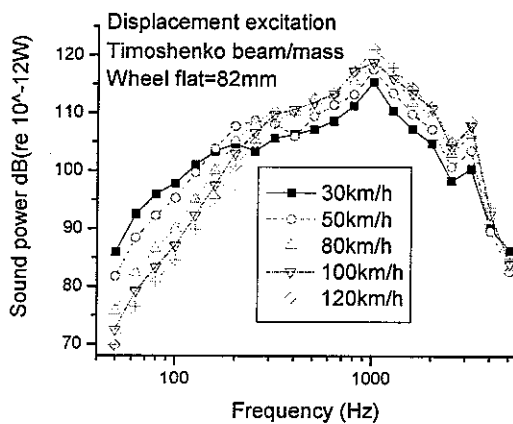


Fig. 8.32 The effect of train speed on noise power.

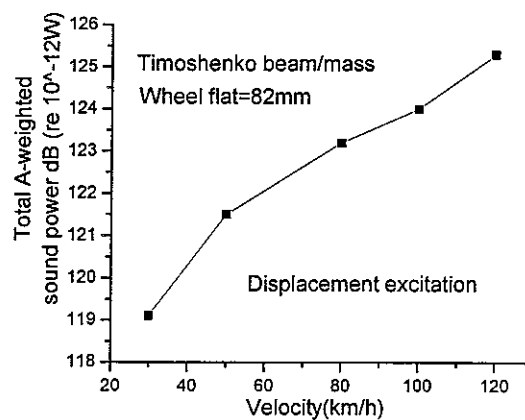


Fig. 8.33 The effect of train speed on total A-weighted noise power.

### 8.4.4 Sound power predicted by Mass/ Timoshenko beam model: the effect of wheel flat length

Figs 8.34 to 8.37 show the effect of wheel flat length on the noise predicted by the mass/Timoshenko beam model under wheel flat displacement excitation at speeds of 30km/h and 80km/h. These results may be compared with Figs 8.22 to 8.25, the results predicted by vehicle/Timoshenko beam with the same kinds of excitation. The vehicle model (either wagon or mass) does not affect the frequency component of noise. There is also no effect on the trend of noise with increasing length of wheel flat. For the total A-weighted sound power, mass model gives less sound power than vehicle model. The difference of total A-weighted between the mass and vehicle model is reduces as the length of wheel flat increases. When the length of wheel flat is 20mm, the difference is 1.8dB, while the difference reduces to 0.4dB when the length of wheel flat is 100mm.

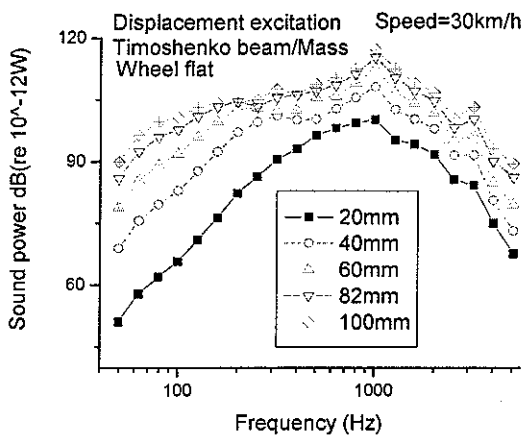


Fig. 8.34 The effect of wheel flat length on noise at speed 30km/h.

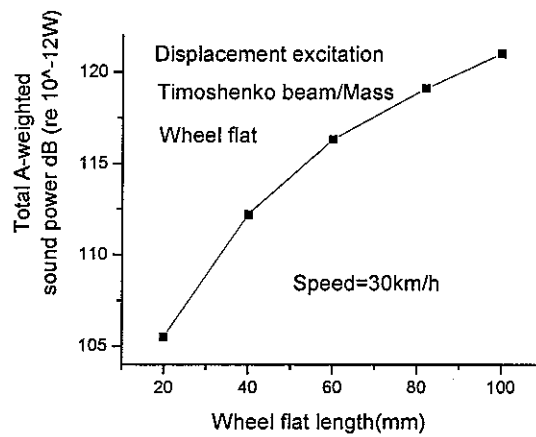


Fig. 8.35 The effect of wheel flat length on total A-weighted noise power at speed 30km/h.

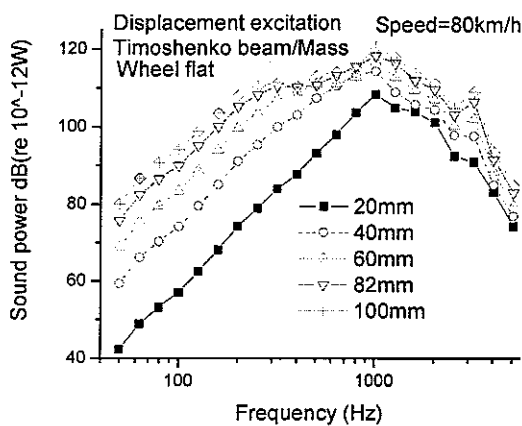


Fig. 8.36 The effect of wheel flat length on noise at speed 80km/h.

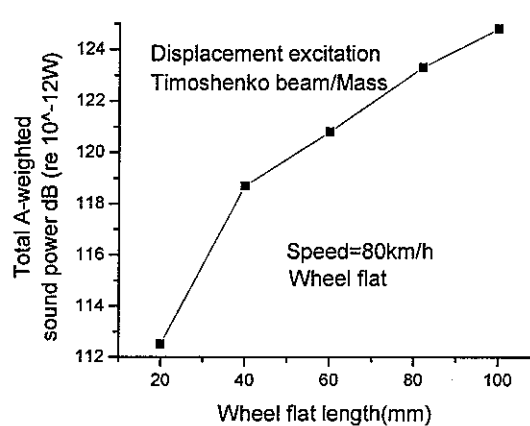


Fig. 8.37 The effect of wheel flat length on total A-weighted noise at speed 80km/h.

## 8.5 Comparison of wheel flat initial velocity and displacement excitation

Figs 8.38 and 8.39 show the noise predicted by the Euler beam model under wheel flat excitation at train speed 30km/h and 80km/h. One model takes the wheel flat as a displacement input and the other transfers the wheel flat into an initial velocity.

Generally speaking, displacement excitation model gives a higher noise in the frequency range from 100Hz to 2500Hz, this frequency range will move toward high frequency as the train speed increase. Beyond this frequency range the initial velocity model give a higher noise level. The frequency at which the maximum noise occurs does not change; that is decided by the beam model.

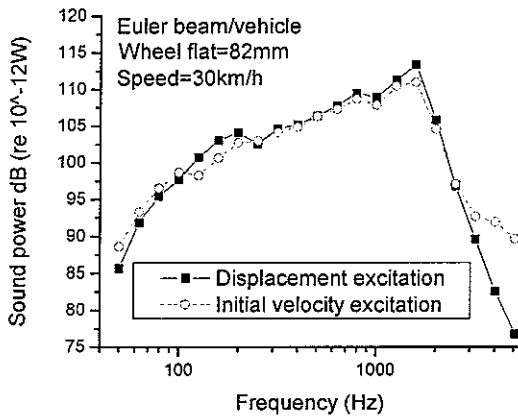


Fig. 8.38 The comparison of noise power produced by two excitation models at speed 30km/h.

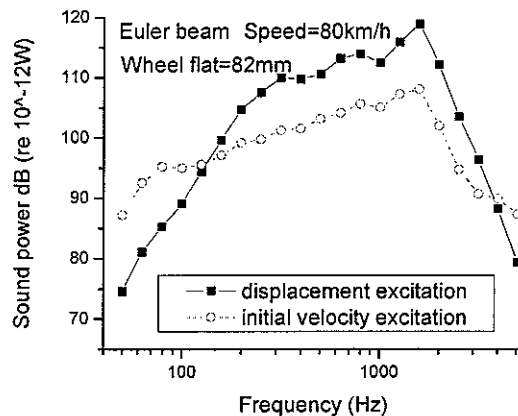


Fig. 8.39 The comparison of noise power produced by two excitation models at speed 80km/h.

## 8.6 Comparison of Euler beam and Timoshenko beam

Figs 8.40 and 8.41 compare the noise predicted by the Euler beam and the Timoshenko beam under wheel flat displacement excitation at train speeds 30km/h and 80km/h.

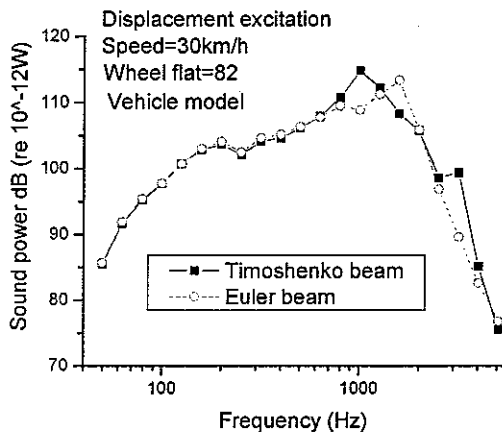


Fig. 8.40 Noise power comparison of Euler beam and Timoshenko beam under wheel flat excitation at train speed 30km/h.

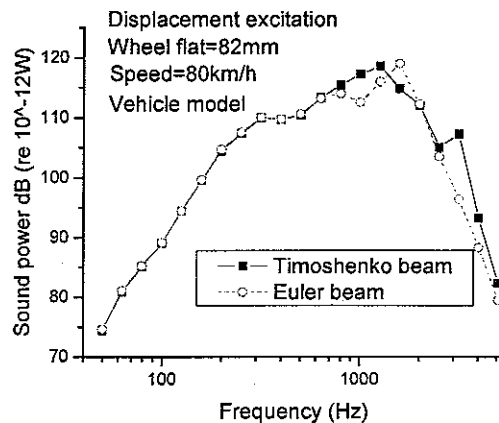


Fig. 8.41 Noise power comparison of Euler beam and Timoshenko beam under wheel flat excitation at train speed 80km/h.

There is little difference between the noise predicted by the Euler beam and the Timoshenko beam below 800Hz. But for frequencies above 800Hz, there are some noticeable differences. One is the frequency which maximum noise happens. The second is that the Timoshenko beam model has a noise peak at 3000Hz, which does not appear in the Euler model. These two phenomena are consistent with the vibration characteristics, which are discussed in the previous chapters.

## 8.7 Comparison of wagon and mass model

Figs 8.42 and 8.43 compare the results for the wagon and mass models of the vehicle. They give the noise predicted by the Timoshenko beam and the Euler beam under wheel flat displacement excitation at a train speed of 80km/h.

From Fig. 8.42 and Fig. 8.43, it can be seen that the choice of vehicle model has little effect on the noise produced by rail vertical vibration.

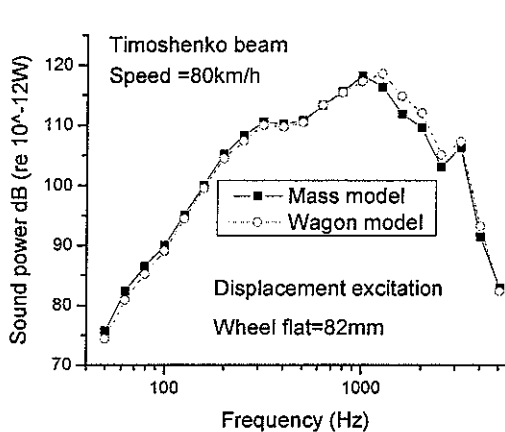


Fig. 8.42 The comparison of noise power produced by wagon and mass model (Timoshenko beam).

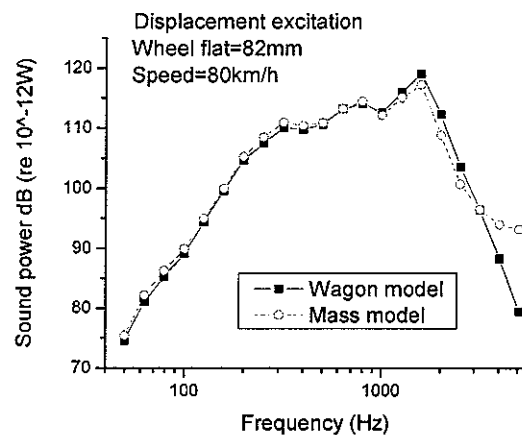


Fig. 8.43 The comparison of noise power produced by wagon and mass model (Euler beam).

For the Timoshenko beam model, the noise difference between the mass and wagon model occurs in the range 1000Hz to 2500Hz. The noise produced by the wagon model is about 2dB higher than the mass model result. At other frequencies the difference in noise is less than 1dB. For the Euler beam model, except the difference described above, at high frequency, above 3200Hz, the mass model gives higher noise than the wagon model, the difference being 14dB at 5000Hz.

## 8.8 Dipped rail joint excitation

### 8.8.1 Sound power predicted by vehicle/ Euler beam model: the effect of train speed

In this section the noise is predicted for excitation due to a dipped joint. First the vehicle/Euler beam model is used, and then the Timoshenko beam is used to replace the Euler beam.

Fig. 8.44 gives the noise spectra for different train speeds. Fig. 8.45 shows the effect of train speed on total A-weighted noise. From Fig. 8.44, it can be seen the effect of speed on noise for the dipped joint rail is similar to the effect of speed on noise with the initial velocity wheel flat excitation that is shown in Fig. 8.2.

The noise increases as train speed increases for the whole frequency range, and total A-weighted sound power increases as train speed increases. The effect of speed on noise by the dipped joint rail is different with the wheel flat excitation, which has a highest sound power at middle speed (for initial velocity excitation, it is about 30km/h).

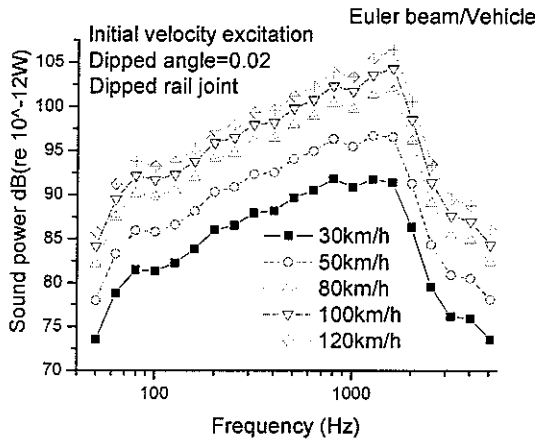


Fig. 8.44 The effect of train speed on noise.

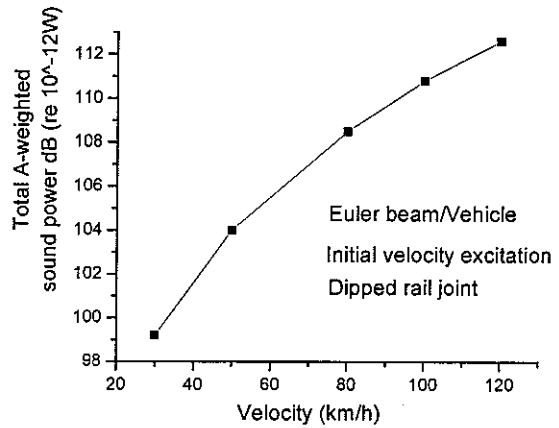


Fig. 8.45 The effect of train speed on total A-weighted noise.

### 8.8.2 Sound power predicted by vehicle / Timoshenko beam model: the effect of train speed

When the Euler beam is changed into a Timoshenko beam, the noise predicted is as shown in Fig. 8.46. It is again very similar to the same model with the initial velocity wheel flat excitation. The noise in the whole frequency range increases as the speed increases. The maximum noise occurs at frequency of 1000Hz. The total A-weighted sound power increases as the train speed increases.

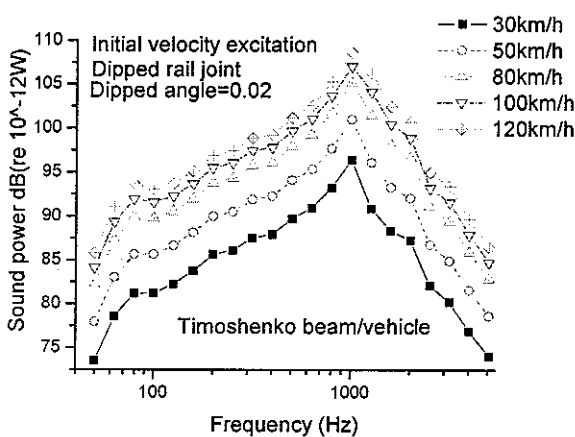


Fig. 8.46 The effect of train speed on noise power.

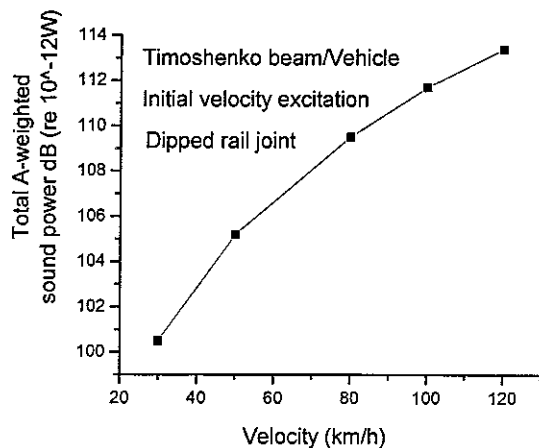


Fig. 8.47 The effect of train speed on total A-weighted noise power.

### 8.8.3 Sound power predicted by vehicle / Timoshenko beam model: the effect of dipped angle

The effect of dipped angle on noise is calculated by taking a fixed train speed of 30km/h, and varying the dipped angle. The results are shown in Figs 8.48 and 8.49. From Fig. 8.48, it is clear that the noise, for all frequencies, increases as the dipped angle increases. The total A-weighted noise varies 13.1dB when the dipped angle changes from 0.02 to 0.08 rad. It increases by slightly more than 6dB for a doubling of angle.

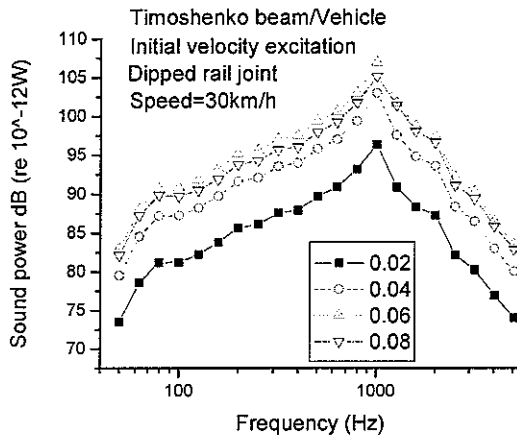


Fig. 8.48 The effect of dipped angle on noise power.

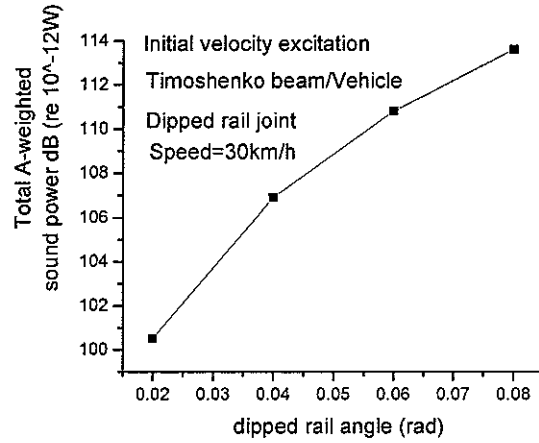


Fig. 8.49 The effect of dipped angle on total A-weighted noise power.

## 9 Conclusions

1 With the initial velocity excitation model of the wheel flat the maximum noise level happens at a train speed of about 30km/h. At that speed the wheel/rail contact force is also maximum. For the displacement excitation model, however the noise and force will continue to increase as train speed increases, although more slowly.

2 When the excitation is modelled as an initial velocity, the train speed and the length of the wheel flat do not affect the shape of the noise spectra; they only change the amplitude of noise.

3 In the displacement excitation model of the wheel flat, the low frequency component of noise will reduce as the train speed increases, but at high frequency, the noise increases as the train speed increases.

4 The frequency of maximum noise is determined by the rail model. For the Timoshenko beam model, the frequency is 1000Hz, but for the Euler beam model it is 1600Hz. In the Timoshenko beam model with displacement excitation, there is another noise peak at 3000Hz that does not appear in the Euler beam model.

5 The vehicle model and excitation model do not affect the frequency at which the noise caused by rail vertical vibration is maximum.

6 The Euler beam model can be used reliably to predict the noise for frequencies up to 800Hz.

7 The mass model of the vehicle can be used to predict the rail noise for frequencies below 1000Hz. This frequency range enlarges to 5000Hz if the rail is modelled as a Timoshenko beam. Even between 1000Hz to 2500Hz, there is only a 2 dB error compared with the full vehicle model.

## 10 References

1. A.Cai, G.P.Raymond, Theoretical model for dynamic wheel/rail and track interaction. In: International Wheelset Congress, Sydney, Australia, 1992, pp.127-131.
2. W.Zhai, X.Sun, A detailed model for investigating interaction between railway vehicle and track. In: Proc. 13<sup>th</sup> IAVSD Symp., 1993. pp.603-614.
3. B.Ripke, and K.Knothe, Simulation of high frequency wagon-track interactions. Vehicle Syst. Dyn. Supplement 24, pp.72-85.
4. W.Zhai, Vehicle-Track Coupling Dynamics. China Railway Press, Beijing. (In Chinese) 1997
5. Y.Q.Sun, and M. Dhanasekar, A dynamic model for the vertical interaction of the rail track and wagon system. International Journal of Solids and Structures, 39(2002), pp.1337-1359.
6. Y.Satoh, Dynamic effect of a flat wheel on track deformation. Bulletin of International Railway Congress Association, 1965, 42(8/9), pp547-553.
7. T.X.Wu, and D.J.Thompson, A hybrid model for the noise generation due to railway wheel flats. Journal of Sound and Vibration. (2002) 251(1), pp115-139.
8. D.J.Thompson, C.J.C. Jones and N. Turner, Investigation into the validity of two-dimensional models for sound radiation from waves in rails. Journal of the Acoustical Society of America. 113(4) ,1965-1974(2003).

# Appendix

## A.1 Rail parameters

Rail	Cross-Section area	Second moment of area	Mass per unit length
UIC 60	$76.9 \times 10^{-4} \text{ m}^2$	$30.55 \times 10^{-6} \text{ m}^4$	60.4 kg/m

## A.2 Parameters under the rail

Stiffness (N/m)				Damping (Ns/m)				Mass (kg)	Note
Pad	Ballast	Bed	Ballast shear	Pad	Ballast	Bed	Ballast shear	Sleeper	
$3.5 \times 10^8$	$4.9 \times 10^7$	$(8.6 \times 10^9)$	$(7.84 \times 10^9)$	$\eta=0.25$ $(1.24 \times 10^5)$	$\eta=1.0$ $(5.88 \times 10^4)$	$(3.12 \times 10^4)$	$(8.0 \times 10^4)$	162	[7]

Note: the data in brackets are used in this calculation.

## A.3 Vehicle or mass-spring parameters

C62a	Mass of body (kg)	Mass of frame (kg)	Mass of wheelset (kg)	Body moment of inertia(kg.m <sup>2</sup> )	Frame moment of inertia(kg.m <sup>2</sup> )	Secondary suspension stiffness (N/m)	Secondary suspension damping (N.s/m)
	77000	1100	1200	$1.26 \times 10^6$	760.0	$5.32 \times 10^6$	$7.0 \times 10^4$

Mass-spring	Mass of upper mass (kg)	Mass of lower mass (kg)	Stiffness (N/m)	Damping (N.s/m)
	600.0	3.0	$5.0 \times 10^9$	$1.95 \times 10^5$